

## Reviewer Comments

In my original review I wrote:

.... my overall rating is major revisions because of two points emphasized here:

– ....

– Some numbers in Table 2 needs to be checked, the mean and median IWC and, *especially, the mean and median of Ntotal for CC are too high for natural cirrus* – see comment 20). This number is definitely not ok, obviously contrails are mixed in the natural cirrus class.

Here is the specific point of my review:

### Point 20 c)

Mean/median of Ntotal for CC are **6.06/3.75** cm<sup>-3</sup>. This is too high for natural cirrus. From Voigt et al. (2017), I would expect something around **0.1** cm<sup>-3</sup> or even lower.

And here is the answer to it:

PSD of natural cirrus are significantly different according to measurement location and the different probes used. Here, the new clustering method shows lower number concentrations for the “natural cirrus”.

In the new manuscript one finds:

Mean/median of Ntotal for CC are **5.092 / 3.444** cm<sup>-3</sup>

which is nearly the same as before (and not lower !!) - and it is still much too high (see the plot below), so the authors didn't take this major comment seriously.

Wrt the argument that N\_ice greatly vary with measurement location: yes, but observations > 1 cm<sup>-3</sup> are exceptions, and unrealistic as mean or median values at any location....

In the middle plot (Voigt et al. 2017, ML-Cirrus, 18 hours of N\_ice observations) you can see that already a value of 1 cm<sup>-3</sup> is rarely exceeded. During ML-Cirrus lots of contrails were observed, representing almost all higher values in the Figure, in natural cirrus the frequency of cirrus with N\_ice > 1 cm<sup>-3</sup> is much smaller. Voigt et al. (2017):

In Table 3, the median of Ntotal of AC1 (Aged Contrail 1) is 1,696 cm<sup>-3</sup>, while in CC it is 3,444 cm<sup>-3</sup>. Also, the 25% and 75% percentiles are lower for AC1 than for CC. How can mean/median the ice particle concentrations be lower in aged contrails than in natural cirrus ?

If the mean/median ice particle numbers in CC in Table 3 are not typos (what I thought when I first read the paper), but are now 5.092 / 3.444 cm<sup>-3</sup>, then either the method is called into question (that was the reason that I rated this point as major) or the data base is too small.

How large is the data base, and how much sampling time is spend in the different classes ?

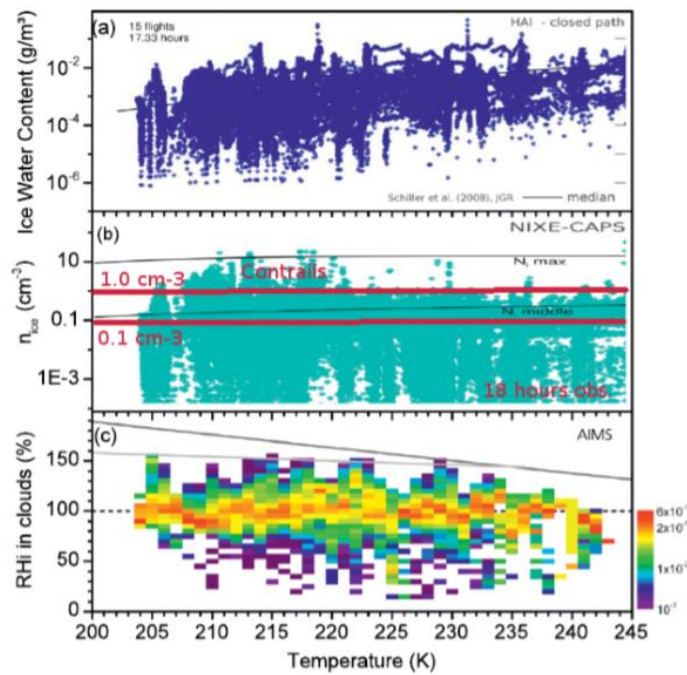


**Fig. 6.** (a) Range and temperature dependence of the IWC detected during ML-CIRRUS derived from HAI/SHARC hygrometers (blue dots) and median from Schiller et al. (2008) (black line). (b) Ice number densities in the size range of 3- to 937- $\mu\text{m}$  diameter ( $N$ ) in cirrus from NIXE-CAPS and middle and maximum  $N$  from Krämer et al. (2009). (c) Relative frequency of RH in cirrus from AIMS-H<sub>2</sub>O (Kaufmann et al. 2016) and Basic Halo Measurement and Sensor System (BAHAMAS) temperature data in 1-K temperature bins. The light gray line shows the homogeneous nucleation threshold from Koop et al. (2000) and the dark gray line shows the liquid water saturation (Murphy and Koop 2005).

#### Answer from authors:

We apologise sincerely to the reviewer for these inaccuracies. We understand his questioning on the microphysical properties of natural cirrus (cluster CC) and will try with this answer to give more details on the previous explanation (l. 655) of the high concentration numbers found in the natural cirrus cluster:

L655: *“However, the ice number concentration and the extinction coefficient are higher than in previous studies, with values around 0.1 cm<sup>-3</sup> and 0.023 km<sup>-1</sup> respectively. Besides to interpolation between the FSSP-300 and the 2DC measurements, the assumed shape (spherical or aspherical), and shattering of large ice particles in cirrus and aged contrails can also have a significant effect on the measurement of optical and microphysical properties (Gayet et al., 2012).”*

First, as mentioned previously in the manuscript, the accuracies on microphysical parameters derived from both FSSP-300 and 2D-C probes are seriously hampered by the combination of inherent limitations of these two old probe versions. The effects of shattering of large ice particles (typically larger than 100  $\mu\text{m}$ ) on FSSP probe tips may significantly increase the number concentration of small particles (see among others Febvre et al., 2009) whereas the use of the 2D-C at Falcon airspeed ( $\sim 180 \text{ m s}^{-1}$ ) lead to large sizing and counting errors (for size lower than 100  $\mu\text{m}$ ) due to optical and electronic limitations (Lawson et al., 2006).

The Particle size distribution of Cluster CC now called PC (polluted cirrus, in blue) on figure 7 shows high concentrations of ice crystals in the 2D-C size range (from 50 to 800  $\mu\text{m}$ ). Shattering of

large ice crystals on the FSSP and 2DC probe tips may result in a significant increase of the concentration of small particles in the FSSP size range and a decrease of the number concentration in the 2D-C size range. Indeed, our results show that high particle concentrations (even higher than AC1 cluster) are found in the FSSP size range (between 0,5 and 18  $\mu\text{m}$ ) which is not in agreement with previous studies on cirrus microphysical properties (Voigt et al., 2017 for instance).

New instruments (such as CDP, 2D-S, CAS ...) can now be equipped with new tips designed to greatly reduce the production of ice fragments from shattering (Korolev et al., 2011). Software techniques detecting closely spaced particles (inter arrival time) assumed to result from shattering are also available to account for shattering contamination of the measurements. Unfortunately, our measurements were based on “old” instruments for which these techniques were not (or couldn't be) applied. Whereas the shattering of large ice crystals should not be significant in contrails, it could have strongly impacted our measurements in cirrus clouds (CC cluster). This effect is now discussed thoroughly in the text and number concentration values for ice crystals with size larger than 50  $\mu\text{m}$  are also mentioned.

Secondly, as mentioned in the manuscript, the interpolation technique used to derive PSD in the 17  $\mu\text{m}$  – 50  $\mu\text{m}$  size range, not accurately measured by the FSSP nor the 2DC, can also lead to large uncertainties in the derived number concentration. Voigt et al., 2017 showed that particles in this size range account for one third of the total concentration measured in natural cirrus and contrail cirrus (see figure 7).

*I. 704: “A linear interpolation in logarithmic space is applied for each PSD in the size range from 17  $\mu\text{m}$  to 50  $\mu\text{m}$  to cover the gap from 17  $\mu\text{m}$  to 50  $\mu\text{m}$ . Because of this gap, the derived microphysical properties should be considered with caution, but may be used to check the cluster definitions.”*

Our results still show that the PCA combined with a K-means classification can be used to clearly discriminate young from aged contrails based on their scattering properties only. This method is thus an interesting approach to analyse the contrail evolution. However, with this dataset, the method cannot clearly separate the scattering properties of aged contrails from the natural cirrus properties. Cluster CC presents significant NO concentrations with microphysical properties close to aged contrails, and we cannot exclude that the higher ice number densities in the cirrus compared to the mean in Voigt et al., 2017 might be explained by an aviation impact. Therefore, the term “natural cirrus” should be changed to “polluted cirrus”. This has been modified in the text after having discussed the results in Figure 6. Indeed, the cirrus observed during CONCERT 1 and 2 could have been influenced by aviation with high traffic density over Germany.

To answer the last question of the reviewer, the number of used cases per cluster for the microphysical property calculations (need to have both complete FSSP and 2DC measurements), are:

- Cluster PW: 482 points
- Cluster YC1: 141 points
- Cluster YC2: 2369 points
- Cluster AC1: 6833 points
- Cluster AC2: 470 points
- Cluster CC: 1655 points

The corresponding times spent on each cluster are difficult to retrieve due to the mixing of data from 8 flights. However, 1 point corresponds to 1 second of measurements. Thus, cluster CC and AC1 have a sufficient number of data points to derive mean values for the measured properties in both clusters.

## Modifications:

In the all text, “natural cirrus” has been replaced by “cirrus” (cluster CC). Then, NO studies allow characterizing “cirrus” as “polluted cirrus” (cluster PC). Because two different clusters can be defined between “aged contrail” and “polluted cirrus” from the k-mean clustering method, these two clusters are still studied separately.

l. 229: *“These equations do not account for possible shattering of large ice crystals on the probe inlets. This effect is minor in young contrails but can lead to an underestimation of large ice crystal concentration (diameters higher than 100  $\mu\text{m}$ ) and thus an overestimation of small ice crystal concentration in contrail cirrus clouds (Febvre et al., 2009).”*

l. 565: *“Due to the high and similar nitrogen oxide concentrations in clusters AC1 and CC, we can conclude that the clouds initially classified as “natural cirrus” are, in fact, significantly influenced by high-density air traffic over Germany. In what follows, these parts of CONCERT measurements are classified as “polluted cirrus” (cluster PC).”*

l. 605: *“In addition, the differences observed between the PSD of PW/YC1/YC2 and AC1/AC2/PC can be explained by the production of small ice crystals (from 1 to 10  $\mu\text{m}$ ) in fresh exhaust plumes followed by rapid dilution during subsequent minutes after the exhaust. It is important to note that aged contrail measurements classified into the AC1 cluster present significantly lower ice particle concentrations than polluted cirrus. The small differences between the two clusters in optical and chemical properties may be explained by strong shattering effects, as mentioned previously. Indeed, the shattering of large ice particles (diameters larger than 100  $\mu\text{m}$ ) can increase the particle number concentrations significantly (Febvre et al., 2009).”*

l. 613: *“Even if shattering effects influence ice particle concentrations within the 2DC range, the PSDs are still consistent with the cluster definitions.”*

l. 642: *“Cluster PC corresponds to polluted cirrus. The IWC is significantly higher (28  $\text{mg m}^{-3}$ ) within this cluster than in other clusters, and higher than observed in previous studies for clean natural cirrus. Also the ice number concentration and the extinction coefficient for cluster PC are higher than for clean cirrus, with values around 0.1  $\text{cm}^{-3}$  and 0.023  $\text{km}^{-1}$  respectively. As mentioned in section 4.1, cirrus observed during CONCERT campaigns are largely influenced by high-density air traffic over Germany and it is thus still difficult to separate aged-contrails and natural cirrus based on their scattering properties. In addition, shattering effects may have significantly influenced the number concentrations of ice particle as discussed previously (section 2.2). Indeed, if only particles with diameters larger than 50  $\mu\text{m}$  are analysed, which better corresponds to an expected cirrus range, the mean number concentration for the polluted cirrus cluster is 0.001  $\text{cm}^{-3}$ .”*

l. 675: *“However, no strictly clean cirrus has been observed during these two campaigns due to a too strong influence from dense air traffic over Germany.”*

## References:

Febvre, G., Gayet, J.-F., Minikin, A., Schlager, H., Shcherbakov, V., Jourdan, O., Busen, R., Fiebig, M., Kärcher, B. and Schumann, U.: On optical and microphysical characteristics of contrails and cirrus, *Journal of Geophysical Research: Atmospheres* (1984–2012), 114(D2), 2009.

Korolev, A. V., Emery, E. F., Strapp, J. W., Cober, S. G., Isaac, G. A., Wasey, M. and Marcotte, D.: Small ice particles in tropospheric clouds: Fact or artifact? Airborne Icing Instrumentation Evaluation Experiment, *Bulletin of the American Meteorological Society*, 92(8), 967–973, 2011.

Voigt, C., Schumann, U., Minikin, A., Abdelmonem, A., Afchine, A., Borrmann, S., Boettcher, M., Buchholz, B., Bugliaro, L., Costa, A., Curtius, J., Dollner, M., Dörnbrack, A., Dreiling, V., Ebert, V., Ehrlich, A., Fix, A., Forster, L., Frank, F., Fütterer, D., Giez, A., Graf, K., Grooß, J.-U., Groß, S., Heimerl, K., Heinold, B., Hüneke, T., Järvinen, E., Jurkat, T., Kaufmann, S., Kenntner, M., Klingebiel, M., Klimach, T., Kohl, R., Krämer, M., Krisna, T. C., Luebke, A., Mayer, B., Mertes, S., Molleker, S., Petzold, A., Pfeilsticker, K., Port, M., Rapp, M., Reutter, P., Rolf, C., Rose, D., Sauer, D., Schäfler, A., Schlage, R., Schnaiter, M., Schneider, J., Spelten, N., Spichtinger, P., Stock, P., Walser, A., Weigel, R., Weinzierl, B., Wendisch, M., Werner, F., Wernli, H., Wirth, M., Zahn, A., Ziereis, H., and Zöger, M.: ML-CIRRUS - The airborne experiment on natural cirrus and contrail cirrus with the high-altitude long-range research aircraft HALO, *Bulletin of the American Meteorological Society*, doi: 10.1175/BAMS-D-15-00213, 2017.

1 Statistical Analysis of Contrail to Cirrus Evolution during the Contrail and Cirrus Experiments  
2 (CONCERT)

3 Aurélien Chauvigné<sup>1</sup>, Olivier Jourdan<sup>1</sup>, Alfons Schwarzenboeck<sup>1</sup>, Christophe Gourbeyre<sup>1</sup>, Jean  
4 François Gayet<sup>1</sup>, Christiane Voigt<sup>2,3</sup>, Hans Schlager<sup>2</sup>, Stefan Kaufmann<sup>2</sup>, Stephan Borrmann<sup>3,4</sup>,  
5 Sergej Molleker<sup>3,4</sup>, Andreas Minikin<sup>2,5</sup>, Tina Jurkat<sup>2</sup>, Ulrich Schumann<sup>2</sup>

6 <sup>1</sup>Laboratoire de Météorologie Physique, UMR 6016 CNRS/Université Clermont Auvergne,  
7 Clermont-Ferrand, France.

8 <sup>2</sup>Institut für Physik der Atmosphäre, Deutsches Zentrum für Luft- und Raumfahrt (DLR),  
9 Oberpfaffenhofen, Germany.

10 <sup>3</sup>Institut für Physik der Atmosphäre, Universität Mainz, Mainz, Germany.

11 <sup>4</sup>Max-Planck-Institute for Chemistry, Department for Particle Chemistry, Mainz, Germany.

12 <sup>5</sup>Now at: Flugexperimente, Deutsches Zentrum für Luft- und Raumfahrt (DLR), Oberpfaffenhofen,  
13 Germany.

14 **Abstract:**

15 Air traffic affects the cloudiness, and thus the climate, by emitting exhaust gases and particles.  
16 The study of the evolution of contrail properties is very challenging due to the complex interplay of  
17 vortex dynamics and atmospheric environment (e.g. temperature, supersaturation). Despite  
18 substantial progress in recent years, the optical, microphysical, and macrophysical properties of  
19 contrails and ambient cirrus during contrail formation and subsequent ageing are still subject to large  
20 uncertainties due to instrumental and observational limitations and the large number of variables  
21 influencing the contrail life cycle. In this study, various contrail cases corresponding to different  
22 aircraft types and atmospheric conditions are investigated using a statistical method based on the in  
23 situ optical measurements performed during the CONCERT campaigns 2008 and 2011. These two  
24 aircraft campaigns encompass more than 17 aircraft contrail cases. A Principal Component Analysis  
25 (PCA) of the angular scattering coefficients measured by the Polar Nephelometer is implemented.  
26 The goal is to classify the sampled ice cloud measurements in 6 clusters representative of different  
27 contrail development stages (primary wake, young contrail, contrail-cirrus and ~~natural~~-cirrus).  
28 Extinction and, asymmetry coefficients, nitrogen oxide concentrations, relative humidity with respect  
29 to ice (RHI) and particle size distributions are analysed for each cluster to characterize the evolution  
30 of ice-cloud properties during the contrail to cirrus evolution. The PCA demonstrates that contrail  
31 optical properties are well suited to identify and discriminate the different contrail growth stages and  
32 to characterize the evolution of contrail properties.

33 **1 Introduction**

34 Aircraft exhaust plumes have a significant impact on climate and tropospheric chemistry (Lee  
35 et al., 2010; IPCC, 1999). The Intergovernmental Panel for Climate Change IPCC special report on  
36 aviation (1999) estimates that NO<sub>x</sub> emissions from subsonic aircraft increase ozone concentrations at  
37 cruise level. Short and long lived pollution species have different impact on atmospheric chemical  
38 composition depending on the flight level (Frömming et al, 2012). Emissions of water vapour, black  
39 carbon (BC) / soot particles, sulphate (SO<sub>4</sub>) aerosols and nitrogen oxides (NO<sub>x</sub>) contribute to the  
40 modification of the chemical composition of the upper troposphere on shorter timescales (Lee et al.,  
41 2010, Gettelman and Chen, 2013; Liou et al., 2013). The long-term climate impact is mainly driven  
42 by CO<sub>2</sub> emissions. Modelling studies have shown that the direct radiative forcing from aviation is  
43 expected to represent 3-4% (50-60 mW m<sup>-2</sup>) of the anthropogenic forcing (Lee et al., 2010; De Leon

44 et al., 2012) and could reach  $87 \text{ mW m}^{-2}$  in 2025 (Chen and Gettelman, 2016). Aircraft induced  
45 cloudiness has also an important impact on climate, although the quantitative assessment of the  
46 radiative forcing remains a major source of uncertainties (Lee et al., 2010).

### 47 1.1. Contrail formation and evolution

48 Contrail formation is mainly controlled by the thermodynamic properties of the ambient air  
49 and by the aircraft emissions. The conditions for contrail formation can be determined by the Schmidt-  
50 Appleman Criterion (SAC) (Schumann, 1996). Contrail chemical composition can have a significant  
51 impact on the contrail formation (Kärcher et al., 2009). Indeed, the contrail microphysical properties,  
52 as the total number densities and ice crystal diameters, are directly linked to the emission index (e.g.  
53 soot emission index in  $\text{kg-fuel}^{-1}$ ). Several studies in the past have been dedicated to the evolution of  
54 concentrations of nitrogen oxide (NO) and sulphur dioxide (SO<sub>2</sub>) and their oxidized forms (Kärcher  
55 and Voigt, 2006 ; Voigt et al., 2006 ; Schäuble et al., 2009 ; Jurkat et al., 2011).

56 Two different processes of contrail formation have been studied: combustion condensation  
57 trails and aerodynamic condensation trails. Different studies (Gierens and Dilger, 2013; Jansen and  
58 Heymsfield, 2015) have illustrated characteristics of aerodynamically controlled contrail formation  
59 associated to warmer temperatures (observations at temperatures above  $-38^\circ\text{C}$ ). Contrails primarily  
60 initiated by the combustion processes result from the mixing of hot and humid exhaust gases with  
61 cooler and dryer ambient air. This increases the local relative humidity in the exhaust plume leading  
62 to the formation of contrails when the saturation with respect to liquid water is reached. In this case,  
63 soot and sulphate aerosols emitted by the aircraft (Moore et al., 2017) may act as condensation nuclei  
64 to form liquid droplets. Homogeneous ice nucleation of the liquid droplets can occur when the exhaust  
65 cools down through mixing with the ambient temperature, while preserving ice saturation. Small ice  
66 crystals are then formed in the jet phase within some tenths of a second (Kärcher and Yu, 2009).

67 The life-cycle of contrails depends on the interaction with the wake vortices behind aircraft  
68 and the ambient atmosphere (Irvine et al., 2012; Graf et al., 2012; Duda et al., 2013; Carleton et al.,  
69 2013; Schumann and Heymsfield, 2017). The ice crystals in the young contrails are captured within  
70 two counter-rotating wake vortices in the downwash behind the aircraft induced by the aircraft lift,  
71 which induce adiabatic compression, heating, and partial sublimation of the ice crystals within the  
72 primary wake (Lewellen and Lewellen, 2001; Sussmann and Gierens, 2001, Unterstrasser et al., 2008,  
73 Unterstrasser et al., 2016; Kärcher and Voigt, 2017). This primary wake may soon disappear if  
74 ambient air is subsaturated with respect to ice. In the case of supersaturation, the secondary wake  
75 becomes visible, thereby detraining ice particles from the primary wake at a higher level (Sussmann  
76 and Gierens, 1999, Kaufmann et al., 2014). Quasi spherical ice crystals become increasingly  
77 aspherical and grow by uptake of water vapour as long as saturation with respect to ice is prevailing.  
78 In ice saturated conditions, contrails can persist after the vortex breakdown, spread and evolve into  
79 contrail cirrus (Schumann and Heymsfield, 2017). The associated cloud cover (larger than for linear  
80 contrails alone) increases the radiative forcing of contrail cirrus (Burkhardt and Kärcher, 2011;  
81 Schumann et al., 2015).

### 82 1.2. Optical and microphysical properties of contrail phases

83 The assessment of the contrail radiative forcing requires, in particular, an accurate estimation  
84 of the cloud cover, the visible optical depth, the single scattering characteristics, the ice crystal  
85 effective size and habit (Yang et al., 2010; Spangenberg et al., 2013). Satellite observations provide  
86 a comprehensive dataset to study statistically the contrail to cirrus evolution. The combined contrail  
87 tracking algorithms on the Spinning Enhanced Visible and Infrared Imager (SEVIRI) on board the  
88 Meteosat Second Generation (MSG) satellites with properties inferred by the Moderate Imaging



89 Spectroradiometer (MODIS) on board the Terra satellite was used by Vazquez-Navarro et al., (2015)  
90 to characterize the properties of 2300 contrails. Properties included lifetime (mean values of 1h), the  
91 length (130 km), the optical thickness (0.34), the altitude (11.7 km) and the radiative forcing ( $-26 \text{ W}$   
92  $\text{m}^{-2}$  for shortwave forcing over land) of these contrails.

93 However, detailed in situ optical and microphysical measurements are still needed to evaluate  
94 satellite products and to develop more appropriate retrieval algorithm. Discriminating contrails from  
95 natural cirrus from satellite observations remains extremely challenging. Although the optical and  
96 microphysical properties of young contrails (linear contrails) differ from natural cirrus properties, the  
97 contrail properties are highly time dependent and persistent contrail cirrus can be embedded in thin  
98 cirrus clouds. Recent *in situ* measurements (Voigt et al., 2017) show that the microphysical properties  
99 of contrail cirrus can still be distinguished from natural cirrus at contrail cirrus ages up to several  
100 hours.

101 Most of the studies (Jessberger et al., 2013; Lewellen et al., 2012 ; Schumann et al., 2013)  
102 separate the contrail analysis between the two wakes. Primary and secondary wake properties depend  
103 strongly on atmospheric conditions and aircraft type (emission index, vortex, flight level, ambient  
104 humidity, temperature, ...). In the primary wake, contrail ice crystals are quasi-spherical with values  
105 of the effective diameter ( $D_{\text{eff}}$ ) typically lower than  $4 \mu\text{m}$  (Schumann et al., 2011; Gayet et al., 2012;  
106 Järvinen et al., 2016; Schumann et al., 2017b). The total number concentration of ice particles is  
107 typically larger than  $1000 \text{ cm}^{-3}$  a few seconds after contrail formation (Baumgardner and Gandrud,  
108 1998; Petzold et al., 1997). Then, it decreases by dilution to concentrations below  $200 \text{ cm}^{-3}$  within  
109 less than a minute after contrail generation (Poellot et al., 1999; Schröder et al., 2000; Gayet et al.,  
110 2012). Gayet et al. (2012) reported mean values of ice water content of  $3 \text{ mg m}^{-3}$  and maximum  
111 extinction coefficients close to  $7 \text{ km}^{-1}$ . In agreement with these results, the recent overview on contrail  
112 studies presented in Schumann et al. (2017b) reports several microphysical properties at different  
113 stages, for different atmospheric conditions as well as comparisons with the Contrail Cirrus Prediction  
114 (CoCIP) model simulations. Their study also highlights a large variability (which increases with  
115 contrail age) of contrail properties.

116 Several studies reported findings on the secondary wake and its evolution into contrail cirrus.  
117 Detrained from the primary wake and submitted to saturated ambient air with respect to ice, ice  
118 crystals grow rapidly, while crystal concentration decreases. Within the first minutes after formation,  
119 measurements exhibit aspherical ice crystals characterized by effective sizes up to  $6 \mu\text{m}$ , IWC ranging  
120 between  $2.5$  and  $10 \text{ mg m}^{-3}$ , extinction between  $2$  and  $3 \text{ km}^{-1}$ , with crystal concentrations typically  
121 lower than  $100 \text{ cm}^{-3}$  (Goodman et al., 1998; Voigt et al., 2010; Kübbeler et al., 2011; Gayet et al.,  
122 2012; Jeßberger et al., 2013; Schumann et al., 2013; Poellot et al., 1999; Febvre et al., 2009;  
123 Kaufmann et al., 2014). Aged contrails can persist and evolve into contrail cirrus if the ambient air is  
124 saturated with respect to ice, however those studies are limited by the lack of unambiguous  
125 identification (Schumann et al., 2017a).

126 After a few minutes, tracking contrails by visual navigation is challenging as contrail and  
127 contrail cirrus spread in the free troposphere. Observations of the ice crystal shape and growth over  
128 several tens of minutes and up to an hour illustrate that crystal effective size can easily reach  $20 \mu\text{m}$   
129 and beyond with number concentrations ranging from  $1$  to  $5 \text{ cm}^{-3}$  (Lawson et al., 1998; Schäuble et  
130 al., 2009), extinction less than  $0.5 \text{ km}^{-1}$  (Febvre et al., 2009), and IWC up to  $10 \text{ mg m}^{-3}$  (Schröder et  
131 al., 2000; De Leon et al., 2012). At this stage, within a sustained ice-supersaturated environment,  
132 contrail microphysical properties may still differ from those of natural cirrus (Voigt et al., 2017) with  
133 concentrations of ice crystals larger than  $100 \mu\text{m}$  in the order of  $0.1 \text{ cm}^{-3}$ . These crystals typically  
134 show bullet rosette type habits (Heymsfield et al., 1998; Heymsfield et al., 2010). Optical depth values  
135 can reach values of  $2.3$  (Atlas and Wang, 2010), corresponding to an extinction of  $0.023 \text{ km}^{-1}$ .



136 Nevertheless, the transition from contrails to cirrus highly depends on the ambient saturation  
137 conditions. Modelling studies with typical atmospheric conditions show a temporal evolution of the  
138 optical and microphysical properties when contrails evolve to contrail cirrus clouds (Burkhardt and  
139 Kärcher, 2011; Unterstrasser et al., 2016 ; Schumann et al., 2015).

140 In this study, we report on a powerful alternative to classify cloud events into young contrail  
141 ~~and; contrail-cirrus-and-natural-cirrus~~. The method is applied to aircraft data of the CONCERT  
142 (Contrail and Cirrus Experiment) campaigns (Voigt et al., 2010, 2011, 2014). The methodology  
143 consists in implementing a Principal Component Analysis (PCA) of the angular light scattering data  
144 measured by the Polar Nephelometer. The PCA patterns are classified to yield different cluster  
145 representing specific contrail types. Corresponding optical, microphysical, and chemical properties  
146 are derived for each contrail phase (from young contrails to cirrus contrails). This paper starts with  
147 an overview of the properties of contrails and cirrus clouds observed during two specific CONCERT  
148 flights (19 November 2008 and 16 September 2011) encompassing a series of different contrail  
149 evolution stages. These two flights containing a variety of contrail-cirrus information can be regarded  
150 as an analytical framework producing results which then can be compared to contrail-cirrus properties  
151 of other flights.

## 152 **2 CONCERT projects and data processing**

### 153 2.1 CONCERT campaigns

154 CONCERT-1 and CONCERT-2 campaigns took place in October/November 2008 and  
155 August/September 2011, respectively. These two campaigns with the DLR Falcon 20 E research  
156 aircraft were based in Oberpfaffenhofen, Germany, and sampled contrails and cirrus at mid-latitudes  
157 over Europe. The overall objective was to reduce uncertainties on the microphysical, chemical, and  
158 radiative properties of contrails behind aircraft of different types and to improve the evaluation of  
159 contrail's impact on climate. A few CONCERT flights were also dedicated to study emissions of Etna  
160 and Stromboli volcanos (Voigt et al., 2014; Shcherbakov et al., 2016). A few stratospheric intrusions  
161 were also observed during the flight missions. In total, 23 flights were recorded during the two  
162 measurement campaigns, wherein 12 flights were entirely focused on aircraft contrail chasing.  
163 Overall, more than 17 different aircraft exhausts plumes have been probed. CONCERT-2 campaign  
164 mainly focused on the observation of persistent contrails, and hence on the evolution of contrails to  
165 contrail cirrus.

166 During both CONCERT campaigns, the DLR research aircraft Falcon was equipped with a  
167 set of instruments to measure the optical and microphysical properties of cloud particles and also the  
168 trace gas composition in the UTLS (Upper Troposphere / Lower Stratosphere) region. Voigt et al.  
169 (2010) provide a detailed description of the aircraft instrumentation. We briefly introduce the  
170 instruments used in this study.

### 171 2.2 Aircraft instrumentation

172 The microphysical and optical particle properties of contrails and cirrus presented in this study  
173 were mainly derived from the PMS Forward Scattering Spectrometer Probe 300 (FSSP-300), the  
174 Polar Nephelometer (PN), and the PMS 2D-C hydrometeor imaging probe. The combination of these  
175 independent techniques characterizes cloud particles within a range of diameters varying from 0.5  
176  $\mu\text{m}$  to 2 mm.

177 The PN (Gayet et al., 1997) measures the angular scattering coefficients (non-normalized  
178 scattering phase function) of an ensemble of water droplets or ice crystals or a mixture of those

179 particles ranging from a few micrometers to approximately 1 mm in diameter. These particles  
 180 intersect a collimated laser beam, at a wavelength of 804 nm, near the focal point of a parabolic  
 181 mirror. The light scattered at angles from 3.49° to 172.5° is reflected onto a circular array of 56 near-  
 182 uniformly positioned photodiodes. In this study, reliable measurements were performed at 30  
 183 scattering angles ranging from ±15° to ±162°. Particle phase (water droplets and/or ice crystals) can  
 184 be assessed as well as single scattering properties such as the extinction coefficient and the asymmetry  
 185 coefficient with uncertainties of 25% and 4%, respectively (Gayet et al., 2002; Jourdan et al., 2010).

186 Particle size distributions and corresponding microphysical and optical integrated properties  
 187 (IWC, Deff, N, and extinction) were derived from both FSSP-300 and 2DC measurements. The FSSP-  
 188 300 (Baumgardner et al., 1992) measures the intensity of forward scattered light from cloud particles  
 189 passing through the laser beam, with cloud particles in the diameter range 0.35-20 μm. In the forward  
 190 angular region (from 4° to 12°), scattering is mainly described by the particle diffraction pattern and  
 191 therefore depends on the refractive index, the shape, and the size of the particles. The method of data  
 192 processing and size calibration used during the CONCERT campaigns have been presented in Gayet  
 193 et al. (2012). We briefly recall that the asymmetry parameter derived from the PN was used to  
 194 discriminate nearly spherical particles ( $g \geq 0.85$ ) from non-spherical ones ( $g < 0.85$ ) at 804 nm. For  
 195 spherical ice particles, Mie calculations were used to derive the size bin limits and the corresponding  
 196 extinction efficiency. Results were adjusted to the calibrated probe response. Additionally, to  
 197 minimize Mie ambiguities related to the FSSP-300 size response, 31 channels were rebinned to 13  
 198 channels with a diameter ranging from 0.5 μm to 18 μm (upper channels 30 and 31 were excluded  
 199 from the data analysis). For non-spherical particles, the size of the contrail particles is expressed in  
 200 terms of an equivalent surface or area diameter, i.e. the diameter of a sphere that has the same area  
 201 than the projected area of the measured non-spherical particle image (Mishchenko et al., 1997;  
 202 Schumann et al., 2011). The particles were assumed to be rotationally symmetric ice ellipsoids with  
 203 an aspect ratio of 0.5. Accordingly, and contrary to the method used for spherical particles, 15 size  
 204 bins ranging from 0.5 μm to 18 μm were defined based on T-Matrix calculations following Borrmann  
 205 et al., (2000).

206 The bi-dimensional optical array spectrometer probe (2DC) provides information on the  
 207 crystal size and shape within a nominal size range from 25 μm to 800 μm by recording cloud particles  
 208 shadow images with a 25 μm resolution. The method of data processing used in this study is described  
 209 in detail in Gayet et al. (2002) and Febvre et al. (2009). Reconstruction of truncated particles has been  
 210 considered for the PSD calculations and the sampling surfaces have been derived according to  
 211 Heymsfield and Parrish (1978). To improve the statistical significance of low particle concentrations,  
 212 a 5-s running mean was applied. As the sensitivity of the probe to small particles decreases with  
 213 airspeed (Lawson et al., 2006), particles smaller than 100 μm may not be detectable at the Falcon  
 214 airspeed of typically 180 m s<sup>-1</sup>. This may result in larger uncertainties of up to 100% in the derived  
 215 microphysical parameters such as the IWC (Gayet et al., 2002 and 2004).

216 For spherical and non-spherical particles, the extinction coefficients are calculated from the  
 217 following equation:

$$Ext = \frac{\pi}{4} \sum_i \beta_{ext}^i N_i D_i^2 \quad (1)$$

218 where  $\beta_{ext}^i$  is the extinction efficiency (values depend on spherical or aspherical particle  
 219 characterization),  $D_i$  the mean diameter in channel  $i$ , and  $N_i$  the number concentration.

220 Different approaches are used to retrieve ice water content from spherical and non-spherical  
 221 particles (Garret et al., 2003 ; Gayet et al., 2004 ; Gayet et al., 2012). For spherical particles (gPN >  
 222 0.85), IWC is computed from the following equation:

$$IWC_{spherical} = \frac{\pi}{6} \rho_{ice} \sum_i N_i D_i^3 \quad (2)$$

223 with  $\rho_{ice}$  the bulk ice density (0.917 g cm<sup>-3</sup>).

224 For non-spherical ice crystals (gPN < 0.85 and for particle diameters larger than 50  $\mu$ m), an  
 225 equivalent diameter method is used (Gayet et al., 2004). For an ice crystal with an area A, the particle  
 226 equivalent diameter  $D_{equ}$  (in mm for eq. (3) and (4)), the equivalent mass  $x_{equ}$  (in mg), and the Ice  
 227 Water Content (IWC in mg m<sup>-3</sup>) are defined as:

$$A \leq 0.049 \text{ mm}^2 \quad D_{equ} = 0.82A^{0.48} \quad (3)$$

$$A > 0.049 \text{ mm}^2 \quad D_{equ} = 0.56A^{0.32} \quad (4)$$

$$x_{equ} = \frac{\pi}{6} \rho_{water} D_{equ}^3 \quad (5)$$

$$IWC_{non-spherical} = \sum_i N_i x_{equ} \quad (6)$$

229 with  $\rho_{water}$  the bulk water density (1 g cm<sup>-3</sup>).

230 These equations do not account for possible shattering of large ice crystals on the probe inlets.  
 231 This effect is minor in young contrails but can lead to an underestimation of large ice crystal  
 232 concentration (diameters higher than 100  $\mu$ m) and thus an overestimation of small ice crystal  
 233 concentration in contrail cirrus clouds (Febvre et al., 2009).

234 Trace gas measurements were also performed. NO/NO<sub>y</sub> concentrations can be significant in  
 235 young tropospheric aircraft plumes. NO and NO<sub>y</sub> mixing ratio were performed using the  
 236 chemiluminescence technique (Schlager et al., 1997) with a time resolution of 1 s. Instruments used  
 237 for CONCERT campaigns are described in several studies (Jurkat et al., 2010 ; Jurkat et al., 2011 ;  
 238 Voigt et al., 2014 ; Jurkat et al., 2016). The accuracy (and precision) of the NO and NO<sub>y</sub>  
 239 measurements are estimated with 7% (and 10%) and 10% (and 15%), respectively (Ziereis et al.,  
 240 2000).

241 Relative humidity with respect to ice (RHI) is also key parameter to understand contrail  
 242 formation and microphysical properties. Water vapour was measured with the chemical ionization  
 243 mass spectrometer AIMS-H<sub>2</sub>O during CONCERT-2 (Kaufmann et al., 2014; 2016). Hygrometers  
 244 using the Lyman- $\alpha$  technique (FISH, Zöger et al., 1999; Meyer et al., 2015), and frost point  
 245 hygrometers (CR-2, Heller et al., 2017) were deployed on the Falcon during CONCERT-1 and 2.

## 246 3 Results

### 247 3.1 Overview of the cloud properties sampled during the reference cases

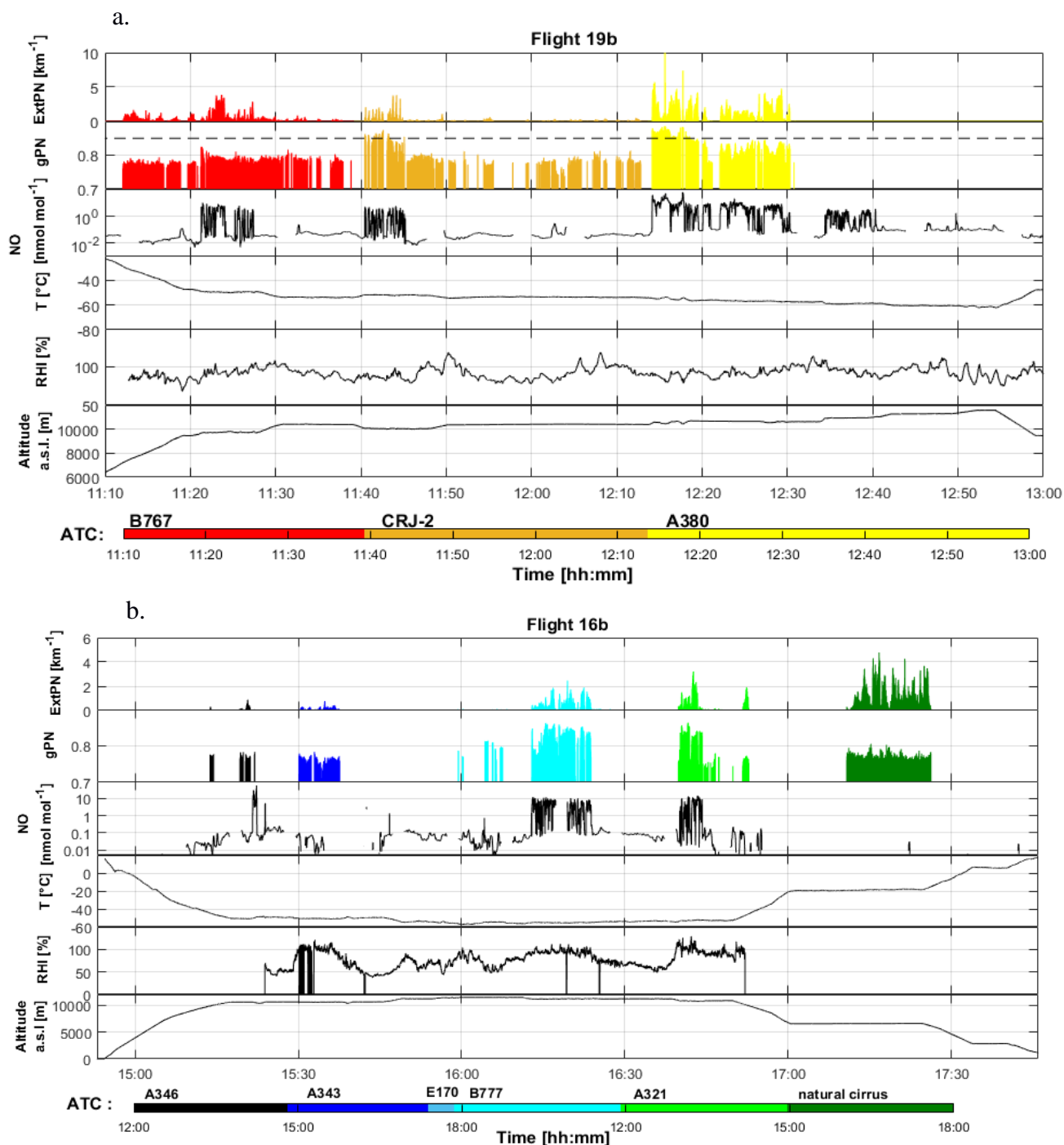


Figure 1: Time series at 1 s resolution for flights a) 19b (CONCERT 1) and b) 16b (CONCERT 2). From top to bottom: extinction coefficient (in km<sup>-1</sup>) and asymmetry parameter measured by the Polar nephelometer at 804 nm (dashed line corresponds to a 0.85 value), concentration of nitric oxide (in nmol mol<sup>-1</sup>) measured by chemiluminescence technique, temperature (in °C), relative humidity with respect to ice (in %), and altitude a.s.l. (in m). Temporal series are coloured according to time and aircraft chasing information from Air Traffic Control (ATC).

248 The purpose of this section is to give an overview of the contrail optical properties and more  
 249 interestingly to evaluate the ability of the Polar Nephelometer measurements to identify contrails.  
 250 Two flights, performed on 16 September 2011 during CONCERT-2 (flight 16b) and on 19 November  
 251 2008 during CONCERT-1 (flight 19b), respectively, were selected for their variety of contrails and  
 252 cirrus sampled during these two flights. The two flights are considered as a benchmark to illustrate  
 253 the potential of the PCA methodology described in Sect. 3.2.

254 Figure 1 displays the time series of the extinction coefficient (ExtPN) and the asymmetry  
255 parameter (gPN) at a wavelength of 804 nm, relative humidity with respect to ice (RHI), the nitric  
256 oxide (NO) concentration, the temperature T and the altitude for flights 19b and 16b. RHI measured  
257 with the AIMS mass spectrometer is shown for flight 16b. RHI measurements during flight 19b as  
258 well as instrument shortcomings are discussed in details in Kübbeler et al. (2011), Gayet et al. (2012),  
259 Jessberger et al. (2013) and Schumann et al. (2013). For both flights, Air Traffic Control (ATC)  
260 provides information on the flight tracks and on the chased aircraft (aircraft type, engine type, fuel  
261 flow, weight, engine power setting). From this information the Falcon measurements were attributed  
262 to the exhaust plume of individual aircraft with an estimated plume age. Time series are colour coded  
263 according to ATC information.

264 The PN extinction coefficient coupled with the asymmetry parameter seems to be a reasonable  
265 proxy to detect contrails and cirrus clouds (see amongst other references, Voigt et al., 2010). ExtPN  
266 values, by definition, depend on the cloud particle concentration and size. Values typically beyond  
267  $0.1 \text{ km}^{-1}$  correspond to cloud events that are well correlated to environmental conditions  
268 supersaturated with respect to ice ( $\text{RHI} > 100\%$ ). Figure 1 shows that relatively high values of  
269 extinction can be found in flights 19b and 16b that are linked to the presence of contrails or cirrus  
270 clouds. Moreover, the temporal distributions of these values are in accordance with ATC information  
271 for both flights. For instance, most of the contrails induced by commercial aircraft exhaust plumes  
272 are associated with significant extinction coefficient values. The ExtPN values are between  $0.2 \text{ km}^{-1}$   
273 and  $10 \text{ km}^{-1}$  for contrails induced by A346, A340, and A380 commercial aircraft. Cirrus clouds are  
274 detected with more variable extinction values mostly larger than  $0.5 \text{ km}^{-1}$ . Most of the aircraft induced  
275 contrails are detected by the PN except for the ones stemming from the E170 airplane. At 15:50 during  
276 flight 16b, ATC identified the E170 position close to the Falcon flight trajectory, however the ExtPN  
277 and the NO mixing ratio remained very low. Hence, the E170 contrail was not probed by the Falcon.  
278 In the following we assume that only periods with ExtPN values above  $0.1 \text{ km}^{-1}$  are considered as a  
279 reliable signature of contrails.

280 The absolute values of the asymmetry parameter gPN provide additional information on the  
281 cloud particle shape. Indeed, gPN is a good indicator of the degree of sphericity of ice crystals (Gayet  
282 et al., 2012). Ice clouds with gPN values higher or equal to 0.85 are typically composed of spherical  
283 ice crystals, whereas lower values are indicative of aspherical ice particles. In a supersaturated  
284 environment, crystals grow by water vapour deposition and become increasingly aspherical with time.  
285 However, in very young contrails, spherical ice crystals with an asymmetry coefficient around 0.85  
286 prevail. gPN is decreasing when water vapour diffusion is generating more and more aspherical  
287 crystal shapes at ice supersaturation. This can be observed for A321 chasing during flight 16b where  
288 gPN is decreasing to a value of 0.75 whilst RHI remains around 100%. This is not the case during  
289 B777 chasing where no gPN decrease is observed when  $\text{RHI} < 100\%$ . However, it is important to  
290 note that the RHI measurements during the CRJ-2 chasing events do not show supersaturated  
291 conditions, whereas contrail seems persistent. Indeed, RHI measurements should be discussed  
292 carefully for this campaign due to calibration issues.

293 Natural cirrus clouds are mainly composed of non-spherical ice crystals. These clouds can be  
294 easily discriminated from young contrails as they exhibit a much lower asymmetry parameter  
295 typically below 0.75 (see amongst others Jourdan et al., 2003b, Febvre et al., 2009). However, no  
296 accurate ambient RHI data can be retrieved for measurements in “natural” cirrus due to instrumental  
297 calibration problems. A good example of the evolution of gPN is the CRJ-2 contrail observed between  
298 11:40 and 11:45 during flight 19b. The sequence illustrates the potential of the gPN measurement to  
299 characterize the evolution of contrail properties. The evolution of the ice crystal shape is reflected in  
300 the decrease of the asymmetry parameter from 0.88 to 0.79 (uncertainties around 0.04) after only 5  
301 min and down to 0.77 after 20 min. A weaker decrease of gPN values (around  $0.78 \pm 0.02$ ) is then



302 observed until 12:10 corresponding to 30 min of contrail ageing. During this period, ice crystals are  
303 expected to grow by water vapour diffusion. A similar decrease of gPN values has been reported by  
304 Gayet et al. (2012) in the ageing contrail from an A380 aircraft, and is also visible in the present study  
305 for the B767 and the A321 contrails.

306 NO concentration measurements can also be used to discriminate natural cirrus clouds from  
307 ice clouds influenced by aircraft traffic. At the typical altitude of 10 km, NO environmental  
308 concentrations are close to background values. In contrast, NO concentrations in young contrails may  
309 reach several tens of  $\text{nmol mol}^{-1}$  (Voigt et al., 2010). Figure 1 shows a good correlation between the  
310 expected localization of young contrails and NO concentrations. The dilution effect in the upper  
311 troposphere causes an important decay of chemical concentrations. For instance, the first few seconds  
312 of the A380 chasing during flight 19b are characterized by a high NO concentration (up to  $40 \text{ nmol mol}^{-1}$ )  
313 followed by a fast decrease to  $10 \text{ nmol mol}^{-1}$  in the next 15 min, and less than  $5 \text{ nmol mol}^{-1}$   
314 beyond 15 min. NO concentrations finally decrease to background levels within hours (e.g. Voigt et  
315 al., 2017). This decrease of the NO concentration is in accordance with the decrease of the extinction  
316 coefficient (from 10 to  $0.2 \text{ km}^{-1}$ ) and asymmetry parameter (from 0.88 to 0.77). NO is mainly used  
317 as an additional contrail indicator. However, during some aircraft chasing events, NO concentrations  
318 were near background levels, while mass spectrometric measurements (not shown here) indicate  
319 elevated concentrations of HONO,  $\text{HNO}_3$ , and  $\text{SO}_2$  representative for contrail chemical species.

320 Flights 19b and 16b clearly show that the optical properties of contrail clouds (supported by  
321 the ATC information) in conjunction with specific trace gas concentration measurements can be used  
322 to discriminate contrails from natural ice cloud events. A first order analysis of these parameters can  
323 be used to roughly distinguish young contrails (mostly quasi-spherical ice crystals) from aged  
324 contrails (mostly aspherical ice crystals) and natural cirrus (background NO concentrations). This  
325 analysis is mainly qualitative and based solely on a few typical parameters (Fig. 1). A more robust  
326 statistical method should be used to accurately separate the different contrail phases ~~from natural~~  
327 ~~cirrus~~. In the following section, relationships between contrail and ice cloud properties scattering  
328 properties are investigated more extensively to assess whether the information content of the PN  
329 scattering measurements is sufficient to document changes in the contrail microphysical properties.

## 330 **3.2 Statistical Method**

331 In this section, we present a methodology based on the statistical analysis of the optical  
332 signature of contrails and cirrus. The goal is to classify the contrail properties according to the  
333 aircraft origin and evolution stage. The main objective of the Principal Component Analysis (PCA)  
334 is data reduction to allow a better physical interpretation of the light scattering patterns derived from  
335 the Polar Nephelometer measurements (Legendre and Legendre, 1998; Jourdan et al., 2003). In this  
336 study, optical properties of ice crystals in the evolving contrail environment are examined to evaluate  
337 contrail evolution. This statistical analysis was already successfully applied to discriminate mixed  
338 phase clouds (Jourdan et al., 2003 ; Jourdan et al., 2010) from liquid clouds and ice clouds, and to  
339 identify porous aerosol in degassing plumes (Shcherbakov et al., 2016).

### 340 **3.2.1 Reference definition**

341 The PCA is first applied to the PN angular scattering coefficients measurements performed  
342 during flights 16b and 19b which are here considered as our reference dataset. Initially, a correlation  
343 matrix is calculated to characterize the link between each scattering angle. The PCA is designed to  
344 generate a new limited set of uncorrelated parameters, called principal components  $C_{ij}$  representative  
345 of the original data set variability.

346 A first implementation of the PCA is performed to detect unreliable data or out of order  
 347 photodiodes. For instance, seven photodiodes presented a low signal to noise ratio and were excluded  
 348 from the dataset. Flight sequences characterized by  $\text{ExtPN} < 0.1$  were also removed. Finally, flight  
 349 sequences dedicated to aircraft chasing and ice cloud sampling were considered to perform a second  
 350 PCA. The analysis is performed on the remaining angular scattering coefficients (4669 Angular  
 351 Scattering Coefficients (ASC) representing PN measurements of flights 16b and 19b) restricted to 25  
 352 angles  $\theta$  ranging from  $15^\circ$  to  $155^\circ$ . The new set of variables or coordinates,  $C_{ij}$ , can be expressed  
 353 with the scalar product of the vector of reduced angular scattering coefficients  $\overrightarrow{\sigma}_j(\theta)$  for the  $j^{\text{th}}$   
 354 measurements, expressed in log scale, and the  $l^{\text{th}}$  eigenvector  $\xi_l(\theta)$  (i.e. principal component) of the  
 355 total data set correlation matrix (Jourdan et al., 2010).

$$C_{ij} = (\overrightarrow{\ln\sigma_j} - \langle \overrightarrow{\ln\sigma} \rangle)^T \cdot \overrightarrow{\xi_l} \quad (4)$$

356 where  $\langle \overrightarrow{\ln\sigma} \rangle$  represents the average ASC of the dataset.

357 The first three eigenvectors  $\overrightarrow{\xi_l(\theta)}$  of the correlation matrix are displayed in Fig. 2 along with  
 358 their normalized eigenvalues  $\lambda_l$ , representing more than 99% of the variability of the PN angular  
 359 scattering coefficients (ASC).

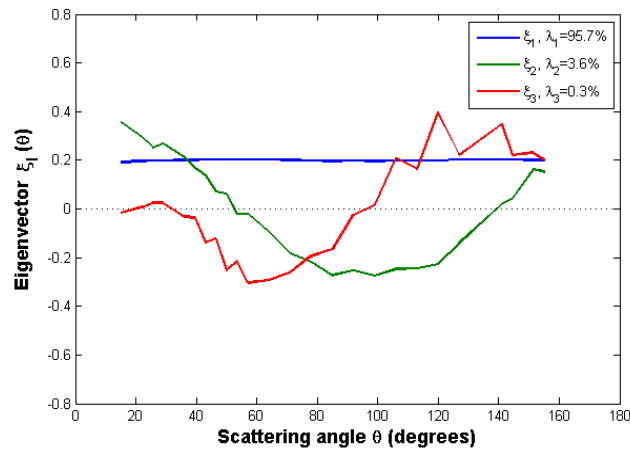


Figure 2: First three eigenvectors for the flights 16b and 19b.

360 The first eigenvector  $\xi_1(\theta)$  is approximately constant versus scattering angle and represents  
 361 95.7% of the total variance. It means that this principal component is representative of changes of the  
 362 magnitude of phase functions without any changes in their global shape. This behaviour means that  
 363 95.7% of the ASC variations are linked to changes of the cloud particle extinction. Results show a  
 364 good correlation ( $r^2 = 0.98$ ) between the first eigenvector and the extinction derived from the PN  
 365 measurements (ExtPN).

366 The second eigenvector  $\xi_2(\theta)$  reverses sign twice at scattering angles equal to  $50^\circ$  and  $140^\circ$   
 367 with an extremum around  $90^\circ$ . Accordingly, 3.6% of the angular scattering variability corresponds to  
 368 a redistribution of scattered energy from the angular region ( $50^\circ$ - $140^\circ$ ) to scattering angles lower than  
 369  $50^\circ$  and higher than  $140^\circ$ . Light-scattering modelling studies demonstrate that the scattering  
 370 behaviour in the angular region between  $60^\circ$  and  $140^\circ$  is sensitive to the particle shape and  
 371 thermodynamic phase (Jourdan et al., 2010). A strong linear correlation ( $r^2=0.97$ ) between the second  
 372 eigenvector and the asymmetry coefficient (gPN) at 804 nm is found.



373 The third eigenvector represents only 0.3% of the total variance. However, this eigenvector  
 374 provides additional information in scattering regions which are not well described by the first two  
 375 principal components. It has opposite signs in the angular region (30°-90°) and (90°-155°) with  
 376 maximum extremal values at 60° and 120°. The shape of the third eigenvector describes the  
 377 forward/backward hemisphere partitioning of the scattering. Baran et al. (2012), Xie et al. (2006),  
 378 and Xie et al. (2009) showed that the scatter pattern for angles between 120° and 160°, corresponding  
 379 to ice bow-like effects, is sensitive to quasi-spherical particles. Moreover, these backscattering angles  
 380 ( $\theta > 120^\circ$ ) and scattering angles around 22° and 46° (corresponding to halo features) can also be linked  
 381 to the particle habits and surface roughness (Xie et al., 2009, Jourdan et al., 2010).

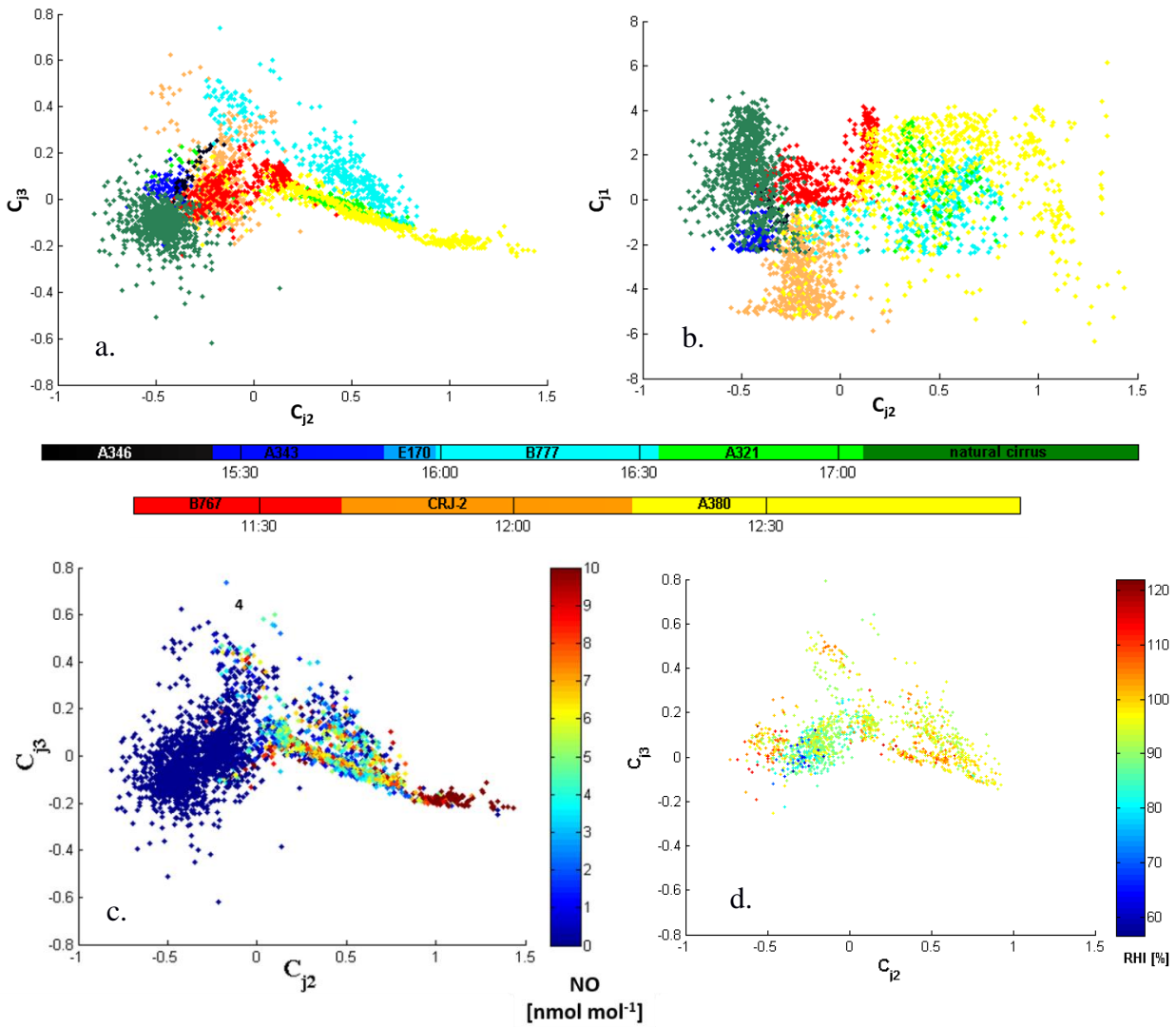


Figure 3: Expansion coefficient diagram for flights 16b and 19b: third versus second principal component for a), c) and d), and first versus second principal component for b). Data points are colour coded according to ATC information for a) and b), by NO concentration for c), and by RHI values for d).

382 Each phase function (or ASC) measured by the PN can be expressed with a good accuracy as  
 383 a linear combination of the three principal components (Jourdan et al., 2010). The PN data are  
 384 projected into a new space defined by the three principal components (3D-space) instead of the 25-  
 385 dimensional space of ASC. The scatterplots of the  $C_{j3}$  and  $C_{j1}$  expansion coefficients versus the  $C_{j2}$   
 386 coefficient are represented on Fig. 3a and b respectively. Fig. 3a illustrates the features of the ASC  
 387 measurements in one of the most comprehensive way. Each point corresponds to a measured phase  
 388 function documented over 25 angles. The variability of  $C_{j2}$  coefficients is significant with values

389 ranging from -1 to 1.5. The angular variation of the second principal component indicates that large  
390 values of  $C_{j2}$  ( $C_{j2} > 0.75$ ) correspond to ASC with low side scattering ( $60^\circ$ - $130^\circ$ ) and higher forward  
391 scattering ( $15^\circ$ - $40^\circ$ ) and somehow higher backscattering ( $145$ - $155^\circ$ ). This behaviour is connected to  
392 an increase of the asymmetry parameter with an increase of  $C_{j2}$  values. Thus, the fraction of spherical  
393 particles increases with increasing  $C_{j2}$ . In the region defined by negative values of  $C_{j2}$  the density of  
394 points is relatively high. These cloud events exhibit optical properties characterized by a large side  
395 scattering and low asymmetry parameter. Therefore, specific cloud sequences sharing similar  
396 scattering properties can be identified based on this second principal component. Young contrails  
397 characterized by quasi-spherical ice crystals have high positive values of  $C_{j2}$  while cirrus clouds and  
398 contrail cirrus exhibit high negative values.

399 In the space of the third principal component high positive values of  $C_{j3}$  imply that less energy  
400 is scattering in the forward hemisphere and thus more energy is scattered in the backward hemisphere.  
401 The variability of the expansion coefficients is less pronounced as ASC are distributed between -0.4  
402 and 0.6. Most of the measured ASC do not significantly differ from the average ASC in the angular  
403 ranges ( $30^\circ$ - $90^\circ$ ) and ( $90^\circ$ - $155^\circ$ ). However, some specific clusters linked to scattering behaviour can  
404 be identified for values of  $C_{j3}$  greater than 0.1 and lower than -0.1. These threshold values also depend  
405 of the position of the ASC on the second principal component. Finally, the first principal component  
406 is directly linked to the extinction coefficient. High values of  $C_{j1}$  are representative of optically dense  
407 cloud sequences.

408 Figure 3c shows an increase of  $C_{j2}$  for increasing NO mixing ratio. This clearly indicates that  
409 the contrails are evolving in space and/or time along the Falcon flight track. Cloud regions influenced  
410 by air traffic can be discriminated from clouds formed by natural processes based on the NO  
411 concentration values. Hence, contrails characterized by a low side scattering due to the presence of  
412 spherical ice crystals correspond to high NO concentration. This behaviour can be a signature of  
413 young contrail properties. Elder or aged contrails composed of a higher fraction of non-spherical  
414 crystals or growing more aspherically are expected to exhibit an enhanced side scattering and a lower  
415 asymmetry parameter associated to lower NO concentrations. RHI measurements also give relevant  
416 information on the capacity of the cloud to be persistent. Thus, Fig. 3d shows higher RHI values with  
417 decreasing gPN values.

### 418 3.2.2 Clustering analyses

419 The new representation of each measurement in the space of the first three principal  
420 component reveals different clusters, characteristic of specific scattering behaviour. The clustering k-  
421 mean method (Seber 1984, Spath 1985) is applied to the reference dataset (flights 19b and 16b) to  
422 partition the observations into k clusters to minimize the variance within each cluster (i.e. to minimize  
423 the distance between each data point and the centre of the cluster it belongs to). The number of cluster  
424 k is an adjustable parameter. Then in a first step, each observation is assigned to a specific cluster  
425 whose mean has the least squared Euclidean distance (i.e. nearest mean). In a second step, the position  
426 of each cluster is set to the mean of all data points belonging to that cluster (i.e. the centroids of each  
427 of the k clusters becomes the new means). These two steps are repeated until convergence is reached  
428 when the assignments no longer change.

429 16 clusters were found to encompass all points of the two flights and to partition each aircraft  
430 chasings identified from ATC information (Fig. 3a and 3b). For clarity and better understanding of  
431 the variability of contrail properties, we choose to limit the number of clusters to 6. 9 clusters are  
432 merged into 2 clusters to define the group “~~natural~~-cirrus” and B767 / A343 / CRJ-2 contrails (referred  
433 hereafter to Cluster 3 and 5 respectively). 4 clusters are also gathered in one new cluster  
434 corresponding to A321 / A380 contrails (referred to Cluster 2 hereafter). In addition, only data within

435 the 10% of the maximum Mahalanobis distance (De Maesschalck et al., 2000) to the respective  
 436 cluster's centre has been considered for this analysis.

437 Clusters are defined by their means (or centres), standard deviations (or widths), and cross-  
 438 correlations (or tilts). The Mahalanobis distance is given by the equation:

$$D_M(x)_i = \sqrt{(x - \mu_i)^T S_i^{-1} (x - \mu_i)} \quad (5)$$

439 with  $D_M$  the Mahalanobis distance between point  $x$  and the  $i^{\text{th}}$  cluster center,  $\mu_i$  the N-dimensional  
 440 mean of this cluster and  $S_i$  its covariance matrix.

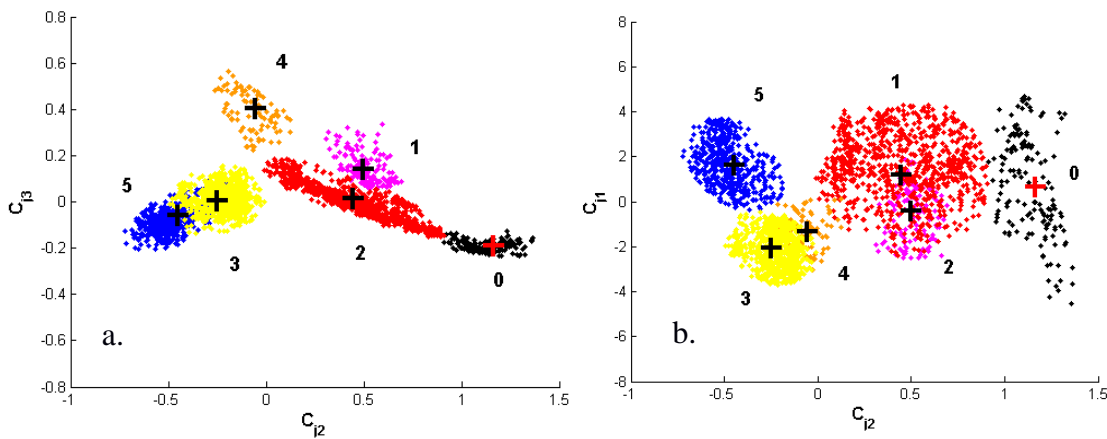


Figure 4: Clustering results of the k-mean method applied to the base (flights 16b and 19b). Third versus second principal component for a), and first versus second principal component for b). Only data within the 10% of the maximum Mahalanobis distance to the respective cluster's centers have been considered for this analyse.

441 Figure 4 shows the partitioning of the dataset into the 6 new clusters (clusters 0 to 5). In the  
 442 following we use data from chemical tracers and optical measurements, and aircraft type information  
 443 to support and discuss the results of the k-means clustering method.

444 While clusters 3 and 5 are characterized by very low NO concentrations (close to zero, Fig.  
 445 3c) above background, clusters 0, 1, 2, and 4 correspond to higher concentrations representative of a  
 446 significant aircraft exhaust influence. ATC information shows that cirrus clouds are gathered in  
 447 cluster 5. Most of the contrails induced by the B767, A343, A346 and CRJ2 aircraft are associated to  
 448 cluster 3 or 5. These cloud events share similar optical properties characterized by a low asymmetry  
 449 parameter, high side scattering behaviour, and supersaturated ambient conditions with respect to ice  
 450 for some cases. Contrails relative to the A380 aircraft are dispatched in cluster 0 and 2 while the ones  
 451 corresponding to the B777 are spread out between clusters 1 and 4.

452 The contrail and cirrus classification based on ASC measurements appears to be consistent  
 453 with the independent trace gas measurements. Each cluster represented on Fig. 4 can be linked to a  
 454 distinct cloud event. Therefore, the combination of flights 16b and 19b can provide a relevant test-  
 455 bed database to discriminate contrail properties. Young contrails (spherical ice crystals) are associated  
 456 to clusters 0, 1 or 2, whereas aged contrails (aspherical ice crystals and high RHI values) with more  
 457 pristine ice are categorized in clusters 3 and 4, and finally ~~natural~~-cirrus (low NO concentrations) are  
 458 found in cluster 5. A less precise analysis (using onboard camera) reveals that cluster 0 corresponds  
 459 essentially to the primary wake created below the secondary wake behind an aircraft. Table 1  
 460 summarizes these cluster's definitions and names used in this work.

Cluster number	definition	name
0	Primary Wake	<b>PW</b>
1	Young Contrail 1	<b>YC1</b>
2	Young Contrail 2	<b>YC2</b>
3	Aged Contrail 1	<b>AC1</b>
4	Aged Contrail 2	<b>AC2</b>
5	Cirrus Cloud	<b>CC</b>

Table 1: Cluster's definitions according to ATC information and tracer measurements (NO concentrations and RHI values)

462 One should keep in mind that some points are still arbitrarily attributed to a particular cluster  
463 without strong physical justification.

### 464 3.2.3 Merging other CONCERT flights

465 In this section we complement the previous analysis with additional cloud optical  
466 measurements performed during other CONCERT flights to increase the robustness of the method.

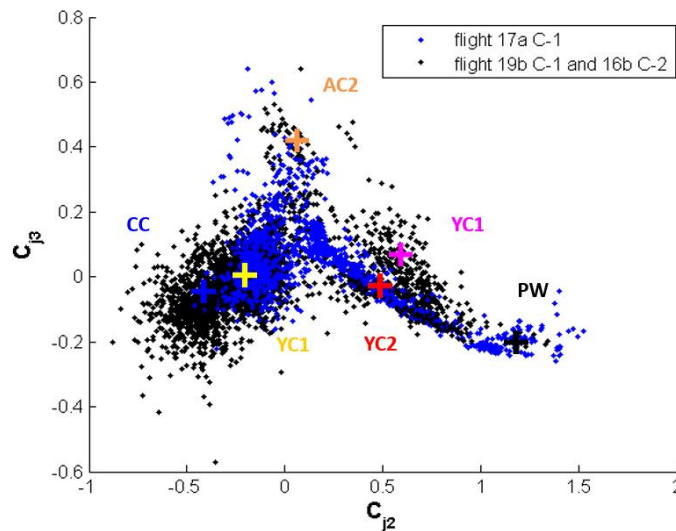


Figure 5: Example of data projection in the  $C_{j2}/C_{j3}$  space where data from flight 17a (blue data points) are superposed on the data from the benchmark flights 19b and 16b (black data points).

467 The ASC measured during other flights can be projected in the space of the principal  
468 components established with flights 16b and 19b dataset. The coordinates of the data points  
469 corresponding to the other flights are calculated from Eq. (4). An example of this data projection is  
470 illustrated in Fig. 5 where flight 17a is represented in the  $C_{j2}/C_{j3}$  space. Each data point can be  
471 attributed to one cluster previously defined by the k-mean clustering method based on flights 16b and  
472 19b dataset (black points). In other words, the ASC measured during another flight can be merged  
473 (projected) into the expansion coefficient diagram displayed on Fig. 3. Data points sharing similar  
474 optical properties will be close to each other on such plot. Figure 5 shows that different contrail phases  
475 are observed during flight 17a. Data points are mostly grouped into cluster AC1, but are also present  
476 in clusters AC2, YC2, and PW. Finally, cloud data gathered during this flight are mainly categorized  
477 as young and aged contrails. We follow this methodology to project and classify each additional

478 “contrail” event performed during both CONCERT campaigns with minimum Mahalanobis distance  
 479 (see Eq. (5)).

Day / Aircraft			Cluster					Number of points	Age (s)	
			PW	YC1	YC2	AC1	AC2			CC
			1st wake	young contrails	aged contrails		Cirrus			
17a C-1	<b>TOTAL</b>						1435			
	A340-311						359	61 - 144		
	<b>TOTAL</b>						2715			
	B737-500						310	77 - 151		
	A340-642						100	82 - 139		
	NC						189	-		
	<b>TOTAL</b>						2152			
	A319-111						628	94 - 129		
	A340-311						175	63 - 90		
	<b>TOTAL</b>						1647			
B767-300						319	77 - 107			
CRJ-2						151	80 - 95			
A380-841						677	109 - 240			
<b>TOTAL</b>						1434				
B737-300						64	90 - 290			
<b>TOTAL</b>						1511				
A340-600						128	100 - 132			
B777						378	120 - 160			
A321						135	70 - 95			
<b>TOTAL</b>						2904				
NC1						498	-			
NC2						233	-			
<b>TOTAL</b>						1380				
B777						371	112 - 178			

Table 2: Classification relative to the six clusters on the Cj2/Cj3 representation of the PCA of all data points for each flight of the two CONCERT campaigns (C-1 in November 2008 and C-2 in September 2011). The legend of the bars represents the relative contribution of data points of individual contrails (blue bars) and also entire flights (black bars) to the 6 individual clusters.

480 The assignment of the data points to the six clusters shown on the expansion diagrams is  
 481 summarized in Table 2. 8 flights (6 additional flights) representing 4426 ASC measurements were  
 482 processed. The lengths of the bars in Table 2 represent the distribution of the data points within the  
 483 different clusters: a) black bars correspond to the fraction of cloud events within a specific flight (with  
 484 extinction coefficient higher than  $0.1 \text{ km}^{-1}$ ) and b) blue bars represent cases of individual contrails  
 485 within the flight. Data points with extinction coefficient lower than  $0.1 \text{ km}^{-1}$  are not shown in the  
 486 table. More than 30% of the data points are located in clusters AC1 and/or CC meaning that they  
 487 correspond to aged contrail and sometimes ~~natural~~-cirrus. Flights clearly performed in well visible  
 488 contrails outside ~~natural~~-cirrus (earlier development stage and/or intensified persistent elder contrails)  
 489 exhibit significant fraction of data points associated to clusters PW, YC1, and YC2 (young contrails)  
 490 for both CONCERT-1 and CONCERT-2 campaigns. However, within these flights data points are  
 491 also gathered in cluster AC1 (aged contrails clean) and to a lesser extent in cluster AC2 (aged  
 492 contrails, mostly corresponding to measurements performed during two different B777 contrail  
 493 chasing events).

494 These results are in reasonable agreement with previous conclusions (this subsection) drawn  
 495 for the cluster definitions and associated contrail / ice cloud characteristics. Very young contrails have  
 496 been mostly chased during CONCERT-1 (flights 19a and 19b). Another interesting result is related  
 497 to flight 17 during CONCERT-2 (flight 17 C-2) where no aircraft information was provided by ATC.  
 498 Still ATC data indicate measurements in exhaust plumes and the Falcon flew apparently in visible



499 contrails ( $\text{ExtPN} > 0.1 \text{ km}^{-1}$ ) which were probably too old for ATC recognition. Our analysis shows  
500 that these data points can mainly be attributed to cluster CC and AC1. This observation suggests that  
501 significantly aged contrails have been sampled. However, crystal formation and growth processes in  
502 contrails and natural cirrus suggest that very old contrails more and more resemble natural cirrus  
503 properties.

504 ATC information on exhaust plume ages was also collected during each chasing. Some  
505 chasings were performed less than 100 s after contrail formation. This is the case for the A340 contrail  
506 during flight 19a and for the CRJ-2 contrail during flight 19b of CONCERT-1 and for the A321  
507 contrail during flight 16b of CONCERT-2. One can notice that the contrail ages are well correlated  
508 to the chosen cluster definitions, revealing that contrail data relative to the A340 are included in  
509 cluster PW and YC2 (young contrails) for more than 90% of the data points, and nearly 63% for the  
510 CRJ-2 and 84% for the A321. According to our cluster classification, only 5% of the data points  
511 gathered during these three flights correspond to aged contrail (cluster AC1 and AC2) categories in  
512 contrast to other CONCERT-1 and CONCERT-2 flights (with more than 30% of data points  
513 associated to AC1 and AC2). Even though it is still difficult to associate contrail ages to measurement  
514 points, the “contrail age” ranges agree with the cluster definitions.

## 515 4 Evolution of contrail properties

### 516 4.1 Optical and chemical cluster properties

517 In the previous section we showed that cloud events can be separated according to their light-  
518 scattering properties. Six clusters were defined based on two flights having a significant number of  
519 data points distributed in each cluster. In this section we present the mean optical, chemical, and  
520 microphysical properties for each cluster. The average properties are calculated for all data points  
521 associated to the 6 individual clusters (all flights, both CONCERT campaigns). Figures 6a, 6c, and  
522 6d show the normalized frequency distributions of the asymmetry parameter (gPN), the extinction  
523 coefficient (ExtPN), and NO concentrations for the six clusters, respectively. Figure 6b represents the  
524 mean normalized scattering phase functions of each clusters. However, it should be noted that the  
525 number of data points could differ significantly from one cluster to another (from 141 measurements  
526 for Cluster YC1 to 8950 measurements for Cluster AC1).

527 The asymmetry parameter gPN statistics shown in Fig. 6a provide the most striking evidence  
528 of the relationship between contrail evolution stage and optical properties. In agreement with findings  
529 of Gayet et al. (2012), aged contrails (cluster AC1 and AC2) and ~~natural~~-cirrus (cluster CC)  
530 correspond to gPN values ranging from 0.72 to 0.80. Younger contrails (cluster YC1 and YC2) have  
531 values of gPN of 0.80 to 0.86. Values of the asymmetry parameter in the primary wake (cluster PW)  
532 are typically above 0.86. These features are a consequence of the time evolution of ice crystal shapes  
533 from quasi-spherical ice particle after exhaust to non-spherical (e.g. column, needle, bullet, and  
534 bullet-rosette type crystals) as the contrail evolves. In the primary wake, the pressure increases in the  
535 descending vortex. This leads to adiabatic heating and subsequent sublimation of the ice crystals  
536 (Lewellen and Lewellen, 2001; Unterstrasser et al., 2016) that can explain the spherical shapes of ice  
537 crystals and thus, the high values of the asymmetry coefficients.

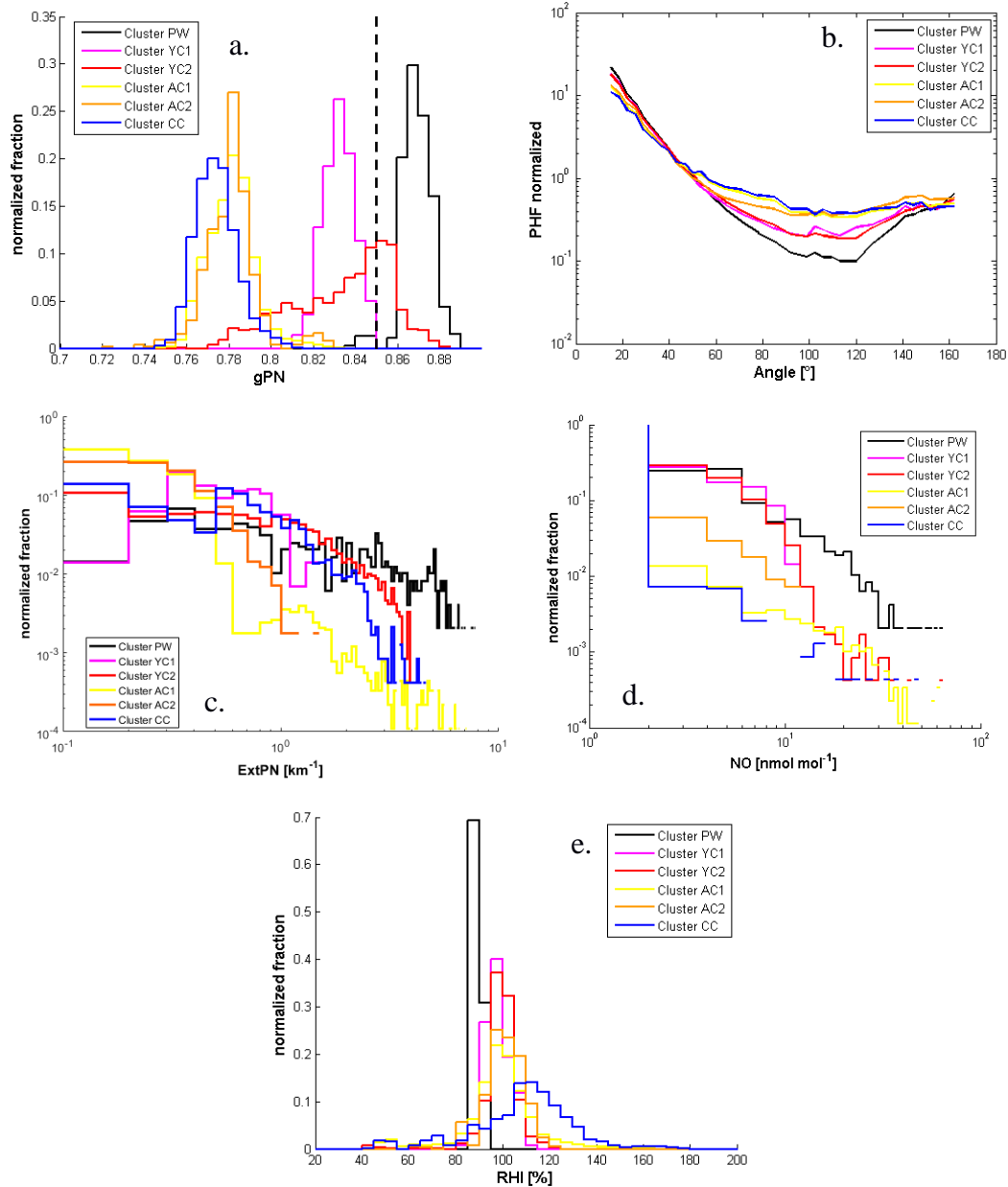


Figure 6: Normalized histograms of a) asymmetry coefficient (dashed line corresponds to a value of 0.85), b) phase function, c) extinction retrieved by Polar Nephelometer, d) NO concentration for all flights, and e) RHI conditions for CONCERT-2 flights.

538 The normalized phase functions are presented in Fig. 6b. Primary wake phase functions  
 539 (cluster PW) are clearly different from the young contrail phase functions (cluster YC1 and YC2),  
 540 which are themselves different from aged contrails (cluster AC1 and AC2) and ~~natural~~-cirrus (cluster  
 541 CC) phase functions. The main difference is observed in the side scattering region (50°-140°). This  
 542 region is related to changes of ice particles shapes and to the fraction of spherical ice crystals within  
 543 the contrails. This behaviour is expected and agrees with the position of clusters PW, YC2 and YC1  
 544 on the expansion coefficient diagram (Fig. 2). Indeed, the decrease of the  $C_{j2}$  coefficient is associated  
 545 to a side scattering enhancement. Therefore, very young contrails are composed mainly of spherical  
 546 ice crystals for which the phase functions indicate a substantial scattering at forward angles and much  
 547 lower scattering at sideward angles. As the contrails evolve, these features smooth out leading to  
 548 phase functions with a featureless flat behaviour at side scattering angles. Finally, the averaged  
 549 normalized phase functions of old contrails and ~~natural~~-cirrus are similar to each other. This also  
 550 explains that they are difficult to discriminate within the PCA.



551 The extinction coefficient statistics are presented in Fig. 6c. All the aged contrails (cluster  
552 AC1 and AC2) exhibit extinction coefficients lower than  $2 \text{ km}^{-1}$ . Also 80% of the sampled ~~natural~~  
553 cirrus (cluster CC) show such low extinction coefficients. For younger contrails (cluster YC1 and  
554 YC2), the extinction coefficients can reach  $5 \text{ km}^{-1}$ . Largest extinction coefficients are found in  
555 primary wake measurements (cluster PW) with values up to  $8 \text{ km}^{-1}$ . Still, the main fraction (more  
556 than 50% of data points) of young contrail data yields extinction coefficients from 0 to  $1 \text{ km}^{-1}$ .

557 Concentrations of chemical species can also be used to characterize contrail/cirrus properties.  
558 The concentration depends strongly on the type of the tracked aircraft. Figure 6d shows the mean  
559 concentration of nitrogen oxide NO for the six individual clusters. Young contrail NO concentrations  
560 (cluster PW, YC1 and YC2) can reach values up to  $10 \text{ nmol mol}^{-1}$  (corresponding to 10% of  
561 measurements). For primary wake measurements (PW in black) a higher concentration can be  
562 reached. Approximately 1% of the data have concentrations close to  $60 \text{ nmol mol}^{-1}$  in the primary  
563 wake. In contrast, in aged contrails and in ~~natural~~-cirrus (cluster AC1, AC2 and CC) NO  
564 concentrations higher than  $2 \text{ nmol mol}^{-1}$  do not exceed 1% of cases. Indeed, after exhaust,  
565 concentrations of nitrogen oxide NO and sulphur dioxide SO<sub>2</sub> created by combustion reactions  
566 decrease rapidly due to the dispersion in the upper troposphere and reactions with other molecules.

567 Due to high and similar nitrogen oxide concentrations in clusters AC1 and CC, we can  
568 conclude that the clouds initially classified as “cirrus” are, in fact, significantly influenced by high-  
569 density air traffic over Germany. In what follows, these parts of CONCERT measurements are  
570 classified as “polluted cirrus” (cluster PC).

571 Finally, saturation conditions with respect to ice are presented in Fig. 6e for all clusters. The  
572 predominant measured ambient relative humidity of all clusters is around 95%. Cluster AC1 and CC  
573 (yellow and blue lines respectively) exhibit median RHI values close to 110% and 120% respectively.  
574 These higher values are suitable for the persistence of the contrail and the formation of cirrus clouds  
575 Supersaturated conditions are not reached for the measurements gathered in the primary wake cluster  
576 (PW). Low humidity values may well occur in primary wakes with non-persisting contrails.

577 These results highlight that the principal component analysis, based on the ASC  
578 measurements described in Sect. 3, can be used to discriminate contrail phases. Specific optical and  
579 chemical properties can thus be derived for each contrail phase and can be related to their evolution.

## 580 4.2 Microphysical cluster properties

581 Microphysical properties are assessed using the combination of FSSP-300 and 2DC  
582 measurements or hydrometeor diameters ranging from  $0.5 \mu\text{m}$  to  $800 \mu\text{m}$ , but with a gap in the size  
583 range  $17 \mu\text{m}$  to  $50 \mu\text{m}$ . Figure 7 shows the averaged number particle size distributions (PSD) for each  
584 cluster and for all flights of the study (8 flights from CONCERT-1 and 2). A linear interpolation in  
585 logarithmic space is applied for each PSD to cover the gap from  $17 \mu\text{m}$  to  $50 \mu\text{m}$ . Because of this  
586 gap, the derived microphysical properties should be considered with caution, but may be used to  
587 check the cluster definitions.

588 PSD measurements in natural cirrus and aged contrails differ significantly depending on the  
589 location of the study, ambient air conditions, measurement methods (instrument limitation (Gayet et  
590 al., 2002), and air speed (Febvre et al., 2009)). Previous studies show that a 3-hours old contrail cirrus  
591 with an effective diameter close to  $20 \mu\text{m}$  (Voigt et al., 2017) and number concentration larger than  
592  $0.1 \text{ cm}^{-3}$  (Schumann et al., 2017) can be composed of ice crystals with sizes up to  $100 \mu\text{m}$  (blue dashed  
593 line, contrail cirrus figure 7). This differs from the PSD of the natural cirrus presented by Voigt et al.  
594 (2017) (dashed black line), which has an order of magnitude lower particle number concentration. In

595 natural cirrus at mid-latitudes, ice crystals with size up to 1600  $\mu\text{m}$  were observed during the ML-  
 596 CIRRUS campaign (dark dashed line Figure 7, Voigt et al., 2017).

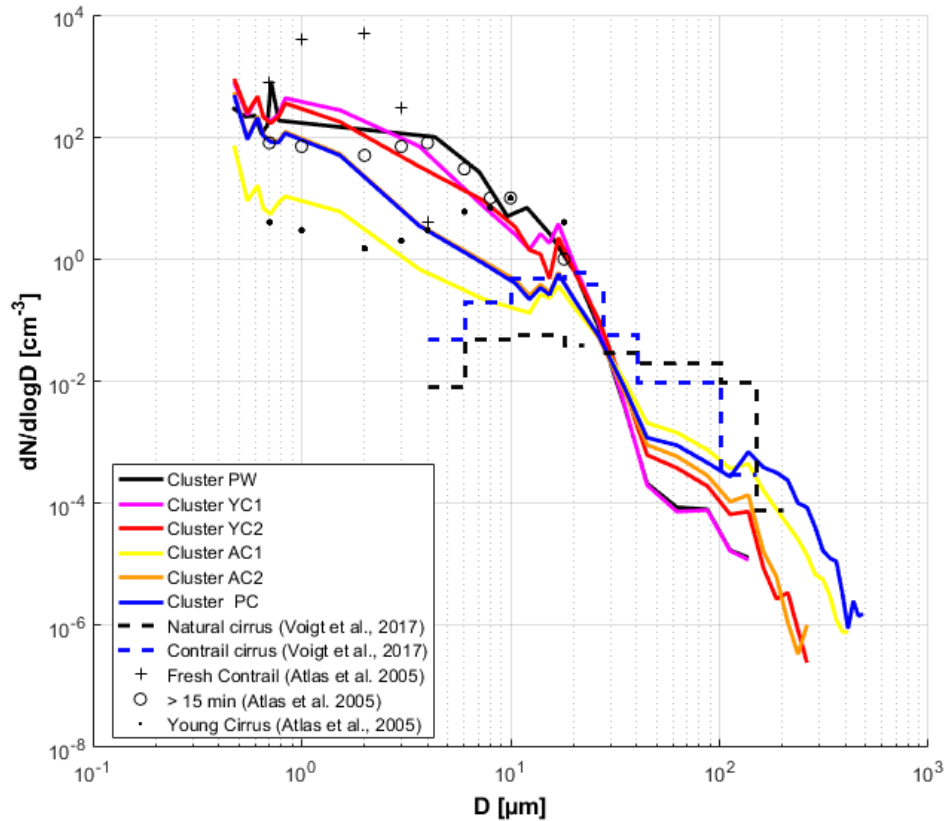


Figure 7: Number particle size distribution for each cluster including all data points of all flights. FSSP-300 measurements from 0.5 to 17  $\mu\text{m}$  and 2DC measurements from 50  $\mu\text{m}$  to 800  $\mu\text{m}$ . The data are linearly interpolated in logarithm space between 17  $\mu\text{m}$  and 50  $\mu\text{m}$ .

597 Figure 7 shows that the mean number PSDs of each cluster are mainly consistent with the  
 598 cluster definition and these previous studies. Indeed, two categories of PSD can be observed. Within  
 599 the FSSP-300 size range, PSD relative to old contrails (cluster AC1 and AC2) and polluted cirrus  
 600 (cluster PC) exhibit number concentration of small ice particles one order of magnitude lower than  
 601 young contrails (clusters YC1 and YC2) and primary wake (cluster PW). Differences in this size  
 602 range should be carefully considered due to uncertainties of the FSSP-300 number concentration  
 603 measurements, which is close to 30% for typical concentrations of  $5\text{cm}^{-3}$  but can reach 75% for  
 604 concentrations of approximately  $0.5\text{cm}^{-3}$  (Gayet et al., 2002). However, we can still discriminate  
 605 primary wake measurements (cluster PW) from secondary wake measurements (clusters YC1 and  
 606 YC2) in the 3 to 10  $\mu\text{m}$  size range.

607 ~~In addition, it is interesting to note that aged contrail measurements classified into AC1~~  
 608 ~~cluster present significantly lower ice particle concentrations than natural cirrus.~~ The differences  
 609 observed between the PSD of PW/YC1/YC2 and AC1/AC2/PC can be explained by the production  
 610 of small ice crystals (from 1 to 10  $\mu\text{m}$ ) in fresh exhaust plumes followed by rapid dilution during  
 611 subsequent minutes after the exhaust. It is important to note that aged contrail measurements  
 612 classified into the AC1 cluster present significantly lower ice particle concentrations than polluted  
 613 cirrus. The small differences between the two clusters in optical and chemical properties may be,  
 614 explained by strong shattering effects, as mentioned previously. - Indeed, the shattering of large ice

615 particles (diameters larger than 100  $\mu\text{m}$ ) can increase the particle number concentrations significantly  
 616 (Febvre et al., 2009).

617 Even if though ice fragments from shattering influence ice particle concentrations in the 2DC size  
 618 range, the PSDs are ~~also still consistent in agreement~~ with the cluster definitions. A higher  
 619 concentration of large ice crystals with diameters around 100  $\mu\text{m}$  and larger are expected for ~~natural~~  
 620 cirrus (cluster PCC) and for significantly well-developed contrails (cluster AC1 and AC2). This is  
 621 particularly well illustrated by the mean PSD from cluster YC1 that displays significantly less  
 622 particles in the 2DC measurements size range than the one corresponding to AC1 and AC2.

Extinction ( $\text{km}^{-1}$ )		Mean	std	Mediane	prctile 25	prctile 75
cluster	PW	4,230	3,820	3,308	1,104	6,485
	YC1	0,720	0,410	0,680	0,351	1,026
	YC2	2,070	2,655	1,017	0,271	2,836
	AC1	0,220	0,484	0,037	0,008	0,158
	AC2	0,110	0,161	0,054	0,004	0,126
	PC	0,370	1,240	0,046	0,001	0,132

IWC ( $\text{mg m}^{-3}$ )		Mean	std	Mediane	prctile 25	prctile 75
cluster	PW	8,173	10,586	5,573	1,665	11,363
	YC1	0,191	0,107	0,168	0,111	0,281
	YC2	4,860	8,918	1,235	0,218	6,604
	AC1	7,072	35,765	0,124	0,000	1,151
	AC2	0,295	1,079	0,094	0,003	0,286
	PC	27,929	144,384	0,126	0,005	0,448

NTOTAL ( $\text{cm}^{-3}$ )		Mean	std	Mediane	prctile 25	prctile 75
cluster	PW	172,965	114,497	152,398	95,564	223,374
	YC1	409,726	205,625	405,127	230,907	603,187
	YC2	188,139	199,736	125,344	52,584	236,100
	AC1	8,206	6,550	1,696	0,966	3,363
	AC2	28,883	43,758	9,176	2,954	42,626
	PC	5,092	24,453	3,444	1,467	6,511

Table 3: Optical and microphysical properties for each cluster according interpolated particle size distributions from FSSP-300 and 2DC measurements.

623 Table 3 presents ice water content (IWC, in  $\text{mg m}^{-3}$ ) and total number of ice crystals  
 624 (NTOTAL, in  $\text{cm}^{-3}$ ) derived from the measured PSD for each cluster. The extinction coefficient (in  
 625  $\text{km}^{-1}$ ) obtained from the PN measurements is also displayed. Despite the large uncertainties associated  
 626 to both instruments and the interpolation between 17  $\mu\text{m}$  and 50  $\mu\text{m}$  diameters, these results again  
 627 show that each cluster can be connected to a specific contrail phase, and their properties can be  
 628 compared to previous studies.

629 In terms of cluster mean values, the microphysical and optical properties of cluster PW agree  
 630 with the cloud properties expected in the primary wakes. The extinction coefficient has a mean value  
 631 of  $4.23 \text{ km}^{-1}$ , IWC is close to  $28 \text{ mg m}^{-3}$ , and the number concentration yields a typical value of 173  
 632 particles  $\text{cm}^{-3}$ . These properties are in agreement with previous measurement reported by Gayet et al.  
 633 (2012) with particle number concentrations close to  $200 \text{ cm}^{-3}$  for contrails less than 60 s after their  
 634 formation. Their work also reports extinction coefficient around  $7 \text{ km}^{-1}$  presenting the highest values  
 635 of the contrail life time.

636 Young (clusters YC1 and YC2) and aged contrails (clusters AC1 and AC2) exhibit distinctive  
637 differences in their extinction coefficients and their concentrations of ice particles. Higher extinction  
638 coefficients and ice number concentration, more than  $0.7 \text{ km}^{-1}$  and  $170 \text{ cm}^{-3}$ , respectively,  
639 characterize young contrails compared to aged contrails, with less than  $0.4 \text{ km}^{-1}$  and around 10  
640 particles  $\text{cm}^{-3}$ , respectively. The ice number concentrations are in agreement with previous results  
641 with values between 200 and  $100 \text{ cm}^{-3}$  for contrail ages between 60 s and 3 min, and around  $5 \text{ cm}^{-3}$   
642 for contrail ages around 10 min (Goodman et al., 1998 ; Lawson et al., 1998 ; Schröder et al., 2000 ;  
643 Schäuble et al., 2009 ; Gayet et al., 2012 ; Voigt et al., 2017). The IWC values differ significantly  
644 between clusters YC1 and YC2 which may be due to a lower number of large particles with diameter  
645 higher than  $20 \mu\text{m}$  in YC1 than in YC2.

646 ~~Cluster PCC corresponds to natural polluted cirrus clouds which experienced strongly~~  
647 ~~variable spreading and ice growth. Indeed, the IWC is significantly higher ( $28 \text{ mg m}^{-3}$ ) within this~~  
648 ~~cluster than in other clusters, and higher than observed in previous studies for clean natural cirrus.~~  
649 ~~Also However, the ice number concentration and the extinction coefficient for cluster PC are higher~~  
650 ~~than for clean cirrus in previous studies, with values around  $0.1 \text{ cm}^{-3}$  and  $0.023 \text{ km}^{-1}$  respectively. As~~  
651 ~~mentioned in section 4.1, cirrus observed during CONCERT campaigns are largely influenced by~~  
652 ~~high-density air traffic over Germany and it is thus still difficult to separate aged-contrails and natural~~  
653 ~~cirrus based on their scattering properties. In addition, shattering effects may have significantly~~  
654 ~~influenced the number concentrations of ice particle as discussed previously (section 2.2). Indeed, if~~  
655 ~~only particles with diameters larger than  $50 \mu\text{m}$  are analysed, which better corresponds to an expected~~  
656 ~~cirrus range Besides to interpolation between the FSSP 300 and the 2DC measurements, the assumed~~  
657 ~~shape (spherical or aspherical), and shattering of large ice particles in cirrus and aged contrails can~~  
658 ~~also have a significant effect on the measurement of optical and microphysical properties (Gayet et~~  
659 ~~al., 2012), the mean number concentration for the polluted cirrus cluster is  $0.001 \text{ cm}^{-3}$ .~~

## 660 Conclusions

661 In this study, a new form of statistical analysis of contrail to cirrus evolution is presented  
662 based on two intensive contrail measurement campaigns, CONCERT-1 and CONCERT-2. The data  
663 are used to study optical and microphysical properties of contrails during their evolution from young  
664 contrails to contrail-cirrus clouds, ~~and of ambient natural cirrus clouds~~. The combination of optical,  
665 microphysical, chemical airborne measurements with aircraft chasing information from ATC was  
666 used to provide an extended view of cloud properties.

667 A Principal Component Analysis (PCA) methodology was applied to the measured Polar  
668 Nephelometer scattering phase function data to facilitate the discrimination of cloud properties of  
669 different contrail phases. The PCA results were derived first for two reference flights that sampled  
670 contrails and cirrus in various development stages, including the primary wake, the young secondary  
671 wake, old contrails (few minutes after formation) and ~~natural polluted~~ cirrus. For these flights, the  
672 PCA clearly demonstrates its potential to discriminate different groups of clouds, justifying the use  
673 of these two flights as a benchmark. Thereafter, the scattering phase functions measured during other  
674 CONCERT flights were projected into the space of principal components obtained from the two  
675 reference flights. Individual data points were assigned to the predefined cluster with minimum  
676 Mahalanobis distances. From the entire data set, the cloud properties in the various contrail  
677 development stages can be analysed separately.

678 The analysis demonstrates that the clearest separation between clusters is derived from  
679 particle shape, which impacts the scattering phase function and the derived asymmetry parameter  
680 gPN. The asymmetry parameter clearly separates young contrails (gPN of 0.72 to 0.80) from  
681 contrail/cirrus with gPN ranging from 0.80 to 0.88. Since the exact contrail age was not always

682 known, young and aged contrails are classified also by their optical and chemical properties. The  
683 measured NO concentrations are also useful to distinguish ~~natural~~-cirrus from old contrails. However,  
684 no strictly clean cirrus has been observed during these two campaigns due to strong influence from  
685 dense air traffic over Germany.

686 Despite the large size gap between the size ranges of the two instruments used, particle size  
687 spectra and related mean values of the ice particle number concentration, extinction and ice water  
688 content have been determined for each cluster. The various clusters clearly show different size  
689 distributions. In good agreement with previous findings on optical and chemical properties, we find  
690 that young contrails have more than a factor of ten higher number concentrations of small ice crystals  
691 (with diameters lower than 20  $\mu\text{m}$ ) than aged contrails ~~and natural cirrus~~. On the other hand, aged  
692 contrails ~~an and polluted cirrus and natural cirrus~~ contain larger ice crystals, with diameters larger  
693 than 75  $\mu\text{m}$ . The optical and microphysical properties of the aged contrail cirrus are often similar to  
694 those found in the ~~ambient~~ “natural/polluted” cirrus clouds. The results show that the PCA method  
695 allows to identify and discriminate different contrail growth stages and to provide an independent  
696 method for the characterization of the evolution of contrail properties.

697 In agreement with Shcherbakov et al. (2016), who characterised volcanic and cirrus using  
698 optical measurements, the PCA method has been clearly shown here to be suitable for contrail studies.  
699 The additional use of microphysical and chemical measurements can be added to the PCA method in  
700 order to improve the selection of contrail phases. Different ranges of extinction or asymmetric  
701 coefficients could be also used for PCA analyses in this perspective. However, additional parameters  
702 should be carefully selected to limit the bias introduced by the limitations of the probes and the  
703 optimal selection may vary from one measurement campaign to another.

704 Accurate modelling of cirrus or contrails’ single scattering properties is required for the  
705 interpretation of remote sensing measurements. Therefore, measurements of the optical  
706 characteristics of ice crystals in natural conditions are still needed for validation of numerical  
707 techniques and for the determination of free parameters in light scattering models. In this context, the  
708 results from the PCA could be used to develop representative parameterizations of the scattering  
709 properties and the ice crystals’ shapes and sizes observed in the visible wavelength range.

## 710 **Acknowledgments**

711 We thank for financial support by the Helmholtz Association under contract VH-NG-309 and  
712 W2/W3-60. Part of this work was funded by DFG SPP HALO 1294 contract VO1504/4-1, and by the  
713 DLR project Eco2Fly in ML-CIRRUS-cirrus special issue. We thank Lufthansa, the DLR flight  
714 department and the Deutsche Flugsicherung for excellent support during the campaign. The in-situ  
715 data can be found in the HALO-database (<https://halo-db.pa.op.dlr.de/>).

## 716 **References**

- 717 Baran, A.J., Gayet, J.-F., and Shcherbakov, V.: On the interpretation of an unusual in-situ measured  
718 ice crystal scattering phase function. *Atmospheric Chemistry and Physics* 12, 9355–9364, 2012.  
719
- 720 Baumgardner, D., Dye, J.E., Gandrud, B.W., and Knollenberg, R.G.: Interpretation of measurements  
721 made by the forward scattering spectrometer probe (FSSP-300) during the Airborne Arctic  
722 Stratospheric Expedition. *Journal of Geophysical Research* 97, 8035–8046, 1992.  
723



- 724 Borrmann, S., Luo, B., and Mishchenko, M.: Application of the T-Matrix Method to the Measurement  
725 of Aspherical (Ellipsoidal) Particles with Forward Scattering Optical Particle Counters. *Journal of*  
726 *Aerosol Science* 31, no. 7 (2000): 789–799, 2000.  
727
- 728 Burkhardt, U., Kärcher, B., and Schumann, U.: Global modeling of the contrail and contrail cirrus  
729 climate impact. *Bulletin of the American Meteorological Society* 91, 479–484, 2010.  
730
- 731 Burkhardt, U. and Kärcher, B.: Global radiative forcing from contrail cirrus. *Nature Climate Change*,  
732 1(1), 54–58, 2011.  
733
- 734 Carleton, A.M., Silva, A.D., Aghazarian, M.S., Bernhardt, J., Travis, D.J., and Allard, J.: Mid-season  
735 climate diagnostics of jet contrail “outbreaks” and implications for eastern US sky-cover trends.  
736 *Climate Research*, 56, 209–230, 2013.  
737
- 738 Chen, C.-C. and Gettelman, A.: Simulated 2050 aviation radiative forcing from contrails and aerosols.  
739 *Atmospheric Chemistry and Physics*, 16(11), 7317–7333, 2016.  
740
- 741 Duda, D. P., Minnis, P., Khlopenkov, K., Chee, T.L., and Boeke, R.: Estimation of 2006 Northern  
742 Hemisphere Contrail Coverage Using MODIS Data. *Geophysical Research Letters*, 40, 612–617,  
743 doi:10.1002/grl.50097, 2013.  
744
- 745 Febvre, G., Gayet, J.-F., Minikin, A., Schlager, H., Shcherbakov, V., Jourdan, O., Busen, R., Fiebig,  
746 M., Kärcher, B., and Schumann, U.: On optical and microphysical characteristics of contrails and  
747 cirrus. *Journal of Geophysical Research: Atmospheres* (1984–2012) 114, 2009.  
748
- 749 Frömming, C., Ponater, M., Dahlmann, K., Grewe, V., Lee, D.S., and Sausen, R.: Aviation-induced  
750 radiative forcing and surface temperature change in dependency of the emission altitude. *Journal*  
751 *of Geophysical Research: Atmospheres* (1984–2012) 117, 2012.  
752
- 753 Gayet, J.F., Crépel, O., Fournol, J.F., and Oshchepkov, S.: A new airborne Polar Nephelometer for  
754 the measurements of optical and microphysical cloud properties. Part I: Theoretical design. In  
755 *Annales Geophysicae*, pp. 451–459, 1997.  
756
- 757 Gayet, J.-F., Auriol, F., Minikin, A., Ström, J., Seifert, M., Krejci, R., Petzold, A., Febvre, G., and  
758 Schumann, U.: Quantitative Measurement of the Microphysical and Optical Properties of Cirrus  
759 Clouds with Four Different in Situ Probes: Evidence of Small Ice Crystals. *Geophysical Research*  
760 *Letters* 29, no. 24: 2230. doi:10.1029/2001GL014342, 2002.  
761
- 762 Gayet, J.-F., Ovarlez J., Shcherbakov, V., Ström, J., Schumann, U., Minikin, A., Auriol, F., Petzold,  
763 A., and Monier M.: Cirrus Cloud Microphysical and Optical Properties at Southern and Northern  
764 Midlatitudes during the INCA Experiment. *Journal of Geophysical Research: Atmospheres* 109,  
765 no. D20 : D20206. doi:10.1029/2004JD004803, 2004.  
766
- 767 Gayet, J.-F., Shcherbakov, V., Voigt, C., Schumann, U., Schäuble, D., Jeßberger, P., Petzold, A.,  
768 Minikin, A., Schlager, H., Dubovik, O., and Lapyonok, T.: The evolution of microphysical and  
769 optical properties of an A380 contrail in the vortex phase. *Atmospheric Chemistry and Physics*. 12,  
770 6629–6643, 2012.  
771
- 772 Garrett, T.J., Gerber, H., Baumgardner, D.G., Twohy, C.H., and Weinstock, E.M.: Small, highly  
773 reflective ice crystals in low-latitude cirrus. *Geophysical Research Letters* 30, 2132, 2003.

774  
775 Guttelman, A., and Chen, C.: The climate impact of aviation aerosols. *Geophysical Research Letters*,  
776 40, 2785–2789, doi:10.1002/grl.50520, 2013.  
777  
778 Gierens, K. and Dilger, F.: A climatology of formation conditions for aerodynamic contrails,  
779 *Atmospheric Chemistry and Physics*, 13, 10847-10857, doi:10.5194/acp-13-10847-2013, 2013.  
780  
781 Graf, K., Schumann, U., Mannstein, H., and Mayer, B.: Aviation induced diurnal North Atlantic cirrus  
782 cover cycle. *Geophysical Research Letters* 39, L16804, doi:10.1029/2012GL052590, 2012.  
783  
784 Goodman, J., Pueschel, R.F., Jensen, E.J., Verma, S., Ferry, G.V., Howard, S.D., Kinne, S.A., and  
785 Baumgardner, D.: Shape and size of contrails ice particles. *Geophysical Research Letters* 25, 1327–  
786 1330, 1998.  
787  
788 Heller, R., Voigt, C., Beaton, S., Dörnbrack, A., Kaufmann, S., Schlager, H., Wagner, J., Young, K.,  
789 and Rapp, M.: Mountain waves modulate the water vapor distribution in the UTLS, *Atmospheric*  
790 *Chemistry and Physics, Discussion*, doi:10.5194/acp-2017-334, in review.  
791  
792 Heymsfield, A.J., and Parrish, J.L.: A computational technique for increasing the effective sampling  
793 volume of the PMS two-dimensional particle size spectrometer. *Journal of Applied Meteorology*  
794 17, 1566–1572, 1978.  
795 Heymsfield, A., Baumgardner, D., DeMott, P., Forster, P., Gierens, K., and Kärcher, B.: Contrail  
796 Microphysics. *Bulletin of the American Meteorological Society* 91, 465–472, 2010.  
797  
798 Irvine, E.A., Hoskins, B.J., and Shine, K.P.: The dependence of contrail formation on the weather  
799 pattern and altitude in the North Atlantic. *Geophysical Research Letters* 39, L12802,  
800 doi:10.1029/2012GL051909, 2012.  
801  
802 Järvinen, E., Schnaiter, M., Mioche, G., Jourdan, O., Shcherbakov, V.N., Costa, A., Afchine, A.,  
803 Krämer, M., Heidelberg, F., Jurkat, T., Voigt, C., Schlager, H., Nichman, L., Gallagher, M., Hirst,  
804 E., Schmitt, C., Bansemer, A., Heymsfield, A., Lawson, P., Tricoli, U., Pfeilsticker, K., Vochezer,  
805 P., Möhler, O., and Leisner, T.: Quasi-spherical Ice in Convective Clouds, *Journal of Atmospheric*  
806 *Sciences*, doi:10.1175/JAS-D-15-0365.1, 2016.  
807  
808 Jansen, J. and Heymsfield, A. J.: Microphysics of aerodynamic contrail formation processes, *Journal*  
809 *of Atmospheric Sciences*, 72(9), 3293–3308, 2015.  
810  
811 Jeßberger, P., Voigt, C., Schumann, U., Sölch, I., Schlager, H., Kaufmann, S., Petzold, A., Schäuble,  
812 D., and Gayet, J.F.: Aircraft type influence on contrail properties, *Atmospheric Chemistry and*  
813 *Physics*, 13, 11965-11984, doi:10.5194/acp-13-11965-2013, 2013.  
814  
815 Jourdan, O., Oshchepkov, S., Gayet, J.-F., Shcherbakov, V., and Isaka, H.: Statistical analysis of  
816 cloud light scattering and microphysical properties obtained from airborne measurements. *Journal*  
817 *of Geophysical Research* 108, 4155, 2003.  
818  
819 Jourdan, O., Mioche, G., Garrett, T.J., Schwarzenböck, A., Vidot, J., Xie, Y., Shcherbakov, V., Yang,  
820 P., and Gayet, J.-F.: Coupling of the microphysical and optical properties of an Arctic nimbostratus  
821 cloud during the ASTAR 2004 experiment: Implications for light-scattering modeling. *Journal of*  
822 *Geophysical Research: Atmospheres* (1984–2012) 115, 2010.  
823



824 Jurkat, T., Voigt, C., Arnold, F., Schlager, H., Aufmhoff, H., Schmale, J., Schneider, J., Lichtenstern,  
825 M., and Dörnbrack, A.: Airborne stratospheric ITCIMS-measurements of SO<sub>2</sub>, HCl, and HNO<sub>3</sub> in  
826 the aged plume of volcano Kasatochi, *Journal of Geophysical Research*, 115, D00L17,  
827 doi:10.1029/2010JD013890, 2010.

828

829 Jurkat, T., Voigt, C., Arnold, F., Schlager, H., Kleffmann, J., Aufmhoff, H., Schäuble, D., Schäfer,  
830 M., and Schumann, U.: Measurements of HONO, NO, NO<sub>y</sub> and SO<sub>2</sub> in aircraft exhaust plumes at  
831 cruise, *Geophysical Research Letters*, 38, L10807, doi:10.1029/2011GL046884, 2011.

832

833 Jurkat, T., Kaufmann, S., Voigt, C., Schäuble, D., Jeßberger, P., and Ziereis, H.: The airborne mass  
834 spectrometer AIMS – Part 2: Measurements of trace gases with stratospheric or tropospheric origin  
835 in the UTLS, *Atmospheric Measurement Technics*, 9, 1907–1923, doi:10.5194/amt-9-1907-2016,  
836 2016.

837

838 Kärcher, B., and Voigt, C.: Formation of nitric acid/water ice particles in cirrus clouds, *Geophysical*  
839 *Research Letters*, 33, L08806, doi:10.1029/2006GL025927, 2006.

840

841 Kärcher, B., and Voigt, C.: Susceptibility of contrail ice crystal numbers to aircraft soot particle  
842 emissions, *Geophysical Research Letters*, 44, 8037-8046, doi:10.1002/2017GL074949, 2017.

843

844 Kärcher, B., and Yu, F.: Role of aircraft soot emissions in contrail formation. *Geophysical Research*  
845 *Letters*, 36, L01804, doi:10.1029/2008GL036649, 2009.

846

847 Kaufmann, S., Voigt, C., Jeßberger, P., Jurkat, T., Schlager, H., Schwarzenboeck, A., Klingebiel, M.,  
848 and Thornberry, T.: In situ measurements of ice saturation in young contrails, *Geophysical*  
849 *Research Letters*, 41, doi:10.1002/2013GL058276, 2014.

850

851 Kaufmann, S., Voigt, C., Jurkat, T., Thornberry, T., Fahey, D. W., Gao, R.-S., Schlage, R., Schäuble,  
852 D., and Zöger, M.: The airborne mass spectrometer AIMS – Part 1: AIMS-H<sub>2</sub>O for UTLS water  
853 vapor measurements, *Atmospheric Measurement Technics*, 9, 939-953, doi:10.5194/amt-9-939-  
854 2016, 2016.

855

856 Kübbeler, M., Hildebrandt, M., Meyer, J., Schiller, C., Hamburger, Th., Jurkat, T., Minikin, A.,  
857 Petzold, A., Rautenhaus, M., Schlager, H., Schumann, U., Voigt, C., Spichtinger, P., Gayet, J.-F.,  
858 Gourbeyre, C., and Krämer, M.: Thin and subvisible cirrus and contrails in a subsaturated  
859 environment, *Atmospheric Chemistry and Physics*, 11, 5853-5865, doi:10.5194/acp-11-5853-  
860 2011, 2011.

861

862 Lawson, R. Paul, Andrew J. Heymsfield, Steven M. Aulenbach, et Tara L. Jensen. « Shapes, sizes  
863 and light scattering properties of ice crystals in cirrus and a persistent contrail during SUCCESS ». *Geophysical research letters* 25, no 9: 1331–1334, 1998.

864

865

866 Lawson, R.P., O'Connor, D., Zmarzly, P., Weaver, K., Baker, B., Mo, Q., and Jonsson, H.: The 2D-  
867 S (stereo) probe: Design and preliminary tests of a new airborne, high-speed, high-resolution  
868 particle imaging probe. *Journal of Atmospheric and Oceanic Technology* 23, 1462–1477, 2006.

869

870 Lee, D.S., Pitari, G., Grewe, V., Gierens, K., Penner, J.E., Petzold, A., Prather, M.J., Schumann, U.,  
871 Bais, A., and Berntsen, T.: Transport impacts on atmosphere and climate: Aviation. *Atmospheric*  
872 *Environment* 44, 4678–4734, 2010.

873

874 Legendre, P., and Legendre, L.: Numerical Ecology, 2nd English ed., 853 pp., Elsevier Science, New  
875 York, 1998.

876

877 De León, R.R., Krämer, M., Lee, D.S., and Thelen, J.C.: Sensitivity of radiative properties of  
878 persistent contrails to the ice water path. *Atmospheric Chemistry and Physics*. 12, 7893–7901,  
879 2012.

880

881 Lewellen, D.C.: Analytic solutions for evolving size distributions of spherical crystals or droplets  
882 undergoing diffusional growth in different regimes. *Journal of the Atmospheric Sciences* 69, 417–  
883 434, 2012.

884

885 Lewellen, D.C., and Lewellen, W.S.: The effects of aircraft wake dynamics on contrail development.  
886 *Journal of the Atmospheric Sciences* 58, 390–406, 2001.

887

888 Liou, K.N., Takano, Y., Yue, Q., and Yang, P.: On the radiative forcing of contrail cirrus  
889 contaminated by black carbon. *Geophysical Research Letters*, 40, 778–784, doi:10.1002/grl.50110,  
890 2013.

891

892 De Maesschalck, R., Jouan-Rimbaud, D., and Massart, D.L.: The Mahalanobis Distance.  
893 *Chemometrics and Intelligent Laboratory Systems* 50, no. 1: 1–18. doi:10.1016/S0169-  
894 7439(99)00047-7, 2010.

895

896 Meyer, J., Rolf, C., Schiller, C., Rohs, S., Spelten, N., Afchine, A., Zöger, M., Sitnikov, N.,  
897 Thornberry, T. D., Rollins, A. W., Bozóki, Z., Tátrai, D., Ebert, V., Kühnreich, B., Mackrodt, P.,  
898 Möhler, O., Saathoff, H., Rosenlof, K. H., and Krämer, M.: Two decades of water vapor  
899 measurements with the FISH fluorescence hygrometer: a review, *Atmospheric Chemistry and*  
900 *Physics*, 15, 8521–8538, doi:10.5194/acp-15-8521-2015, 2015.

901

902 Mishchenko, M.I., Travis, L.D., Kahn, R.A., and West, R.A.: Modeling phase functions for dustlike  
903 tropospheric aerosols using a shape mixture of randomly oriented polydisperse spheroids. *Journal*  
904 *of Geophysical Research* 102, 16831–16, 1997.

905

906 Moore, R. H., Thornhill, K. L., Weinzierl, B., Sauer, D., D’Ascoli, E., Kim, J., Lichtenstern, M.,  
907 Scheibe, M., Beaton, B., Beyersdorf, A. J., Barrick, J., Bulzan, D., Corr, C. A., Crosbie, E., Jurkat,  
908 T., Martin, R., Riddick, D., Shook, M., Slover, G., Voigt, C., White, R., Winstead, E., Yasky, R.,  
909 Ziemba, L. D., Brown, A., Schlager, H., and Anderson, B. E.: Biofuel blending reduces particle  
910 emissions from aircraft engines at cruise conditions, *Nature*, 543, 411-415, 10.1038/nature21420,  
911 2017.

912

913 Schäuble, D., Voigt, C., Kärcher, B., Stock, P., Schlager, H., Krämer, M., Schiller, C., Bauer, R.,  
914 Spelten, N., De Reus, M., Szakáll, M., Borrmann, S., Weers, U., and Peter T.: Airborne  
915 measurements of the nitric acid partitioning in persistent contrails, *Atmospheric Chemistry and*  
916 *Physics*, 9, 8189-8197, 2009.

917

918 Schlager, H., Konopka, P., Schulte, P., Schumann, U., Ziereis, H., Arnold, F., Klemm, M., Hagen,  
919 D.E., Whitefield, P.D., and Ovarlez, J.: In situ observations of air traffic emission signatures in the  
920 North Atlantic flight corridor. *Journal of Geophysical Research* 102, 10739–10, 1997.

921

922 Schröder, F., Kärcher, B., Duroure, C., Ström, J., Petzold, A., Gayet, J.-F., Strauss, B., Wendling, P.,  
923 and Borrmann, S.: On the Transition of Contrails into Cirrus Clouds. *Journal of the Atmospheric*  
924 *Sciences* 57, 464–480, 2000.

925

926 Schumann, U.: On conditions for contrail formation from aircraft exhausts. *Meteorologische*  
927 *Zeitschrift*, 5, 4–23, 1996.

928

929 Schumann, U., and Heymsfield, A.: On the lifecycle of individual contrails and contrail cirrus,  
930 *Meteorological Monographs*, 58, 3.1-3.24, doi: 10.1175/AMSMONOGRAPHS-D-16-0005.1,  
931 2017.

932

933 Schumann, U., Jeßberger, P., and Voigt, C.: Contrail ice particles in aircraft wakes and their climatic  
934 importance, *Geophysical Research Letters*, 40, 2867-2872, doi: 10.1002/grl.50539, 2013.

935

936 Schumann, U., Mayer, B., Gierens, K., Unterstrasser, S., Jessberger, P., Petzold, A., Voigt, C., and  
937 Gayet, J.-F.: Effective Radius of Ice Particles in Cirrus and Contrails. *Journal of the Atmospheric*  
938 *Sciences*, 68, 300–321, 2011.

939

940 Schumann, U., Penner, J.E., Chen, Y., Zhou, C., and Graf, K.: Dehydration effects from contrails in  
941 a coupled contrail-climate model, *Atmospheric Chemistry and Physics*, 15, 11179-11199, doi:  
942 10.5194/acp-15-11179-2015, 2015.

943

944 Schumann, U., Kiemle, C., Schlager, H., Weigel, R., Borrmann, S., D'Amato, F., Krämer, M.,  
945 Matthey, R., Protat, A., Voigt, C., and Volk, C. M.: Long-lived contrails and convective cirrus  
946 above the tropical tropopause, *Atmospheric Chemistry and Physics*, 17, 2311-2346,  
947 doi:10.5194/acp-17-2311-2017, 2017a.

948

949 Schumann, U., Baumann, R., Baumgardner, D., Bedka, S. T., Duda, D. P., Freudenthaler, V., Gayet,  
950 J.-F., Heymsfield, A. J., Minnis, P., Quante, M., Raschke, E., Schlager, H., Vázquez-Navarro, M.,  
951 Voigt, C. and Wang, Z.: Properties of individual contrails: a compilation of observations and some  
952 comparisons, *Atmospheric Chemistry and Physics*, 17(1), 403–438, doi:10.5194/acp-17-403-2017,  
953 2017b.

954

955 Seber, G. A. F.: *Multivariate analysis of variance and covariance. Multivariate observations*, 433–  
956 495, 1984.

957

958 Shcherbakov, V., Jourdan, O., Voigt, C., Gayet, J.F., Chauvigne, A., Schwarzenboeck, A., Minikin,  
959 A., Klingebiel, M., Weigel, R., Borrmann, S., Jurkat, T., Kaufmann, S., Schlage, R., Gourdoyre,  
960 C., Febvre, G., Lapyonok, T., Frey, W., Molleker, S., and Weinzierl, B.: Porous Aerosol in  
961 Degassing Plumes of Mt. Etna and Mt. Stromboli. *Atmospheric Chemistry Physics* 16, no. 18:  
962 11883–97. doi:10.5194/acp-16-11883-2016, 2016.

963

964 Spath, Helmuth. *The Cluster Dissection and Analysis Theory FORTRAN Programs Examples*.  
965 Prentice-Hall, Inc., 1985.

966

967 Sussmann, R., and Gierens, K.M.: Lidar and numerical studies on the different evolution of vortex  
968 pair and secondary wake in young contrails. *Journal of Geophysical Research: Atmospheres* 104,  
969 2131–2142, 1999.

970

- 971 Sussmann, R., and Gierens, K.M.: Differences in early contrail evolution of two-engine versus four-  
972 engine aircraft: Lidar measurements and numerical simulations. *Journal of Geophysical Research:*  
973 *Atmospheres* 106, 4899–4911, 2001.  
974
- 975 Vazquez-Navarro, M., Mannstein, H. and Kox, S.: Contrail life cycle and properties from 1 year of  
976 MSG/SEVIRI rapid-scan images, *Atmospheric Chemistry and Physics*, 15(15), 8739–8749, 2015.  
977
- 978 Voigt C., Schlager, H., Ziereis, H., Kärcher, B., Luo, B.P., Schiller, C., Krämer, M., Popp, P.J., Irie,  
979 H., and Kondo, Y.: Nitric acid in cirrus clouds, *Geophysical Research Letters*, 33, L05803,  
980 doi:10.1029/2005GL025159, 2006.  
981
- 982 Voigt, C., Schumann, U., Jurkat, T., Schäuble, D., Schlager, H., Petzold, A., Gayet, J.-F., Krämer,  
983 M., Schneider, J., Borrmann, S., Schmale, J., Jessberger, P., Hamburger, T., Lichtenstern, M.,  
984 Scheibe, M., Gourbeyre, C., Meyer, J., Kübbeler, M., Frey, W., Kalesse, H., Butler, T., Lawrence,  
985 M.G., Holzäpfel, F., Arnold, F., Wendisch, M., Döpelheuer, A., Gottschaldt, K., Baumann, R.,  
986 Zöger, M., Sölch, I., Rautenhaus, M., and Dörnbrack, A.: In-situ observations of young contrails -  
987 Overview and selected case studies from the CONCERT campaign, *Atmospheric Chemistry and*  
988 *Physics*, 10, 9039–9056, doi:10.5194/acp-10-9039-2010, 2010.  
989
- 990 Voigt, C., Schumann, U., Jessberger, P., Jurkat, T., Petzold, A., Gayet, J.-F., Krämer, M., Thornberry,  
991 T., and Fahey, D.: Extinction and optical depth of contrails, *Geophysical Research Letters*, 38,  
992 L11806, doi:10.1029/2011GL04718, 2011.  
993
- 994 Voigt, C., Jessberger, P., Jurkat, T., Kaufmann, S., Baumann, R., Schlager, H., Bobrowski, N.,  
995 Giuffrida, G., and Salerno, G.: Evolution of CO<sub>2</sub>, SO<sub>2</sub>, HCl, and HNO<sub>3</sub> in the Volcanic Plumes  
996 from Etna. *Geophysical Research Letters*, 41, 6, 2196–2203. doi:10.1002/2013GL058974, 2014.  
997
- 998 Voigt, C., Schumann, U., Minikin, A., Abdelmonem, A., Afchine, A., Borrmann, S., Boettcher, M.,  
999 Buchholz, B., Bugliaro, L., Costa, A., Curtius, J., Dollner, M., Dörnbrack, A., Dreiling, V., Ebert,  
1000 V., Ehrlich, A., Fix, A., Forster, L., Frank, F., Fütterer, D., Giez, A., Graf, K., Groß, J.-U., Groß,  
1001 S., Heimerl, K., Heinold, B., Hüneke, T., Järvinen, E., Jurkat, T., Kaufmann, S., Kenntner, M.,  
1002 Klingebiel, M., Klimach, T., Kohl, R., Krämer, M., Krisna, T. C., Luebke, A., Mayer, B., Mertes,  
1003 S., Molleker, S., Petzold, A., Pfeilsticker, K., Port, M., Rapp, M., Reutter, P., Rolf, C., Rose, D.,  
1004 Sauer, D., Schäfler, A., Schlage, R., Schnaiter, M., Schneider, J., Spelten, N., Spichtinger, P.,  
1005 Stock, P., Walser, A., Weigel, R., Weinzierl, B., Wendisch, M., Werner, F., Wernli, H., Wirth, M.,  
1006 Zahn, A., Ziereis, H., and Zöger, M.: ML-CIRRUS - The airborne experiment on natural cirrus and  
1007 contrail cirrus with the high-altitude long-range research aircraft HALO, *Bulletin of the American*  
1008 *Meteorological Society*, doi: 10.1175/BAMS-D-15-00213, 2017.  
1009
- 1010 Xie, Y., Yang, P., Gao, B.-C., Kattawar, G.W., and Mishchenko, M.I.: Effect of ice crystal shape and  
1011 effective size on snow bidirectional reflectance. *Journal of Quantitative Spectroscopy and*  
1012 *Radiative Transfer* 100, 457–469, 2006.  
1013
- 1014 Xie, Y., Yang, P., Kattawar, G.W., Minnis, P., and Hu, Y.X.: Effect of the inhomogeneity of ice  
1015 crystals on retrieving ice cloud optical thickness and effective particle size. *Journal of Geophysical*  
1016 *Research: Atmospheres* (1984–2012) 114, 2009.  
1017
- 1018 Yang, P., Hong, G., Dessler, A.E., Ou, S.S., Liou, K.-N., and Minnis, P.: Contrails and induced cirrus:  
1019 Optics and radiation. *Bulletin of the American Meteorological Society* 91, 473–478, 2010.  
1020

- 1021 Ziereis, H., Schlager, H., Schulte, P., Velthoven, P. van, and Slemr, F.: Distributions of NO, NO<sub>x</sub>,  
1022 and NO<sub>y</sub> in the upper troposphere and lower stratosphere between 28 and 61 N during POLINAT  
1023 2. *Journal of Geophysical Research: Atmospheres* (1984–2012) 105, 3653–3664, 2000.  
1024
- 1025 Zöger, M., Afchine, A., Eicke, N., Gerhards, M-T., Klein, E., McKenna, D.S., Mörschel, U., Schmidt,  
1026 U., Tan, V., Tuitjer, F., Woyke, T., Schiller, C. : Fast in situ stratospheric hygrometers: A new  
1027 family of balloon-borne and airborne Lyman alpha photofragment fluorescence hygrometers.  
1028 *Journal of Geophysical Research: Atmospheres*, 104, 1807-1816, 1999.  
1029